5-9-2014

Anatomically Realistic Structural Modeling of the Cardiac Purkinje Network: A Basis for Studying Contributions of the Conduction System to Ventricular Arrhythmias

Benjamin Liu

Anatomically Realistic Structural Modeling of the Cardiac Purkinje Network

A Basis for Studying Contributions of the Conduction System to Ventricular Arrhythmias

by

Benjamin Liu

A Thesis Submitted in Partial Fulfillment of the Requirements
for the Degree of Master of Science in Applied and Computational Mathematics
School of Mathematical Sciences, College of Science

Rochester Institute of Technology
Rochester, NY

May 9, 2014

Committee Approval:

R·I·T
College of
Science

Dr. Elizabeth Cherry — Date

School of Mathematical Sciences

Thesis Advisor

Dr. Matthew Hoffman — Date

School of Mathematical Sciences

Committee Member

Dr. David Ross — Date

School of Mathematical Sciences

Committee Member

Dr. Nathan Cahill — Date

School of Mathematical Sciences

Director of Graduate Programs

Abstract

A cardiac arrhythmia is a potentially-lethal event in which the normally orderly electrical activity in the heart is disrupted – it becomes disorganized and compromises effective contraction. To better understand arrhythmia dynamics to develop potential therapies and treatments, experimental, computational, and mathematical tools are required. Simulations of cardiac tissue provide valuable insight into the dynamics of life-threatening cardiac arrhythmias, and though much work has been done in this area, the role of the Purkinje network during ventricular arrhythmias has largely been ignored. The function of the Purkinje network is crucial to normal heart rhythm, so its inclusion into cardiac structural models is a necessary step to furthering our understanding of arrhythmias. Current technological limitations prevent the direct imaging of the intact three-dimensional Purkinje structure, making the incorporation of a Purkinje network into such simulations difficult. At this time most efforts involve generating artificial Purkinje networks either through manual drawing of Purkinje-like structures or through algorithms that generate the structures procedurally based on rules gleaned from physiological studies. Very little work has focused on the incorporation of a Purkinje network based directly on experimental data. Through dissection, photographs of the Purkinje network can be taken, but these two-dimensional photographs do not capture the three-dimensional structure of the network. Here we present a novel method for reconstructing the three-dimensional Purkinje structure based on projecting two-dimensional Purkinje structures recovered from experimental photographs onto realistic ventricular geometries. The resulting three-dimensional Purkinje structures make possible the modeling of the coupled ventricle-Purkinje system. The second major component of our work is the development of two methods by which these systems can be modeled. We implement these models using real anatomical data and find good agreement between the two models and with previous experimental studies. Our work provides a basis for the further study of ventricular arrhythmias, and in particular the role the Purkinje network plays in initiating and maintaining such events.

Acknowledgements

I would like to express my deepest thanks my adviser, Dr. Elizabeth Cherry. Her guidance over the past years has been vital to my development as an applied mathematician. My thesis committee members, Dr. Matthew Hoffman and Dr. David Ross, have both given valuable input in the development of this thesis and I am glad to have been able to work with them on this and other projects. I thank Flavio Fenton for contributing experimental photographs of canine Purkinje networks, a full digitization of the left canine Purkinje network, and for valuable correspondence regarding the digitization of a further Purkinje network. I would like to thank the School of Mathematical Sciences at Rochester Institute of Technology. The community has been a wonderful environment for learning and growing in, and I feel fortunate to have been a part of it. Finally, this work has been supported in part by the National Science Foundation under grant CMMI–1028261, for which we extend our gratitude.

Contents

List of Figures

1 Introduction

Heart disease is a term for a broad class of afflictions of the cardiovascular system; as a leading cause of death worldwide, efforts in many different fields are being made to combat it. While certain types of heart disease are genetic, progressive, or otherwise diagnosable, others, like cardiac arrhythmias, can occur suddenly and without warning, making them very dangerous and difficult to prevent. Cardiac arrhythmias are disruptions in the normal electrical activity of the heart. The heart functions through mechanical contraction, which is a byproduct of electrical excitation of the cardiac tissue. Disruptions in this electrical activity can therefore compromise the contraction of the cardiac muscle, leading to ineffective pumping of blood. While some types of arrhythmias have little noticeable effect, others are potentially lethal and can lead to sudden cardiac death.

Ventricular arrhythmias are especially dangerous because of the critical role the ventricles play in normal heart rhythm. The ventricles are thick, muscular chambers that actively pump blood out of the heart and throughout the body. Ventricular arrhythmias can rapidly become life-threatening if normal electrical activity is not restored, which usually requires the use of aggressive techniques such as defibrillation.

To facilitate the timely and correct sequence of activation of the ventricles, a specialized electrical conduction system called the Purkinje network exists within the ventricles. The Purkinje network functions to distribute stimuli throughout the entire ventricles, leading to a much faster total activation of the ventricles than could be achieved by the spread of excitation solely through the ventricular muscle tissue. The role of the Purkinje network is crucial during normal heart rhythm, but much less is known regarding its function during ventricular arrhythmias. Some experiments have shown that the Purkinje network may be important to the genesis of certain types of arrhythmias [18] and that the absence of the network can alter arrhythmia dynamics [10], but further study is needed to improve our understanding of the effect of the Purkinje network during such events.

Mathematical modeling and computational simulation have become important tools for studying cardiac arrhythmias. While experimentation provides invaluable information regarding the behavior of the physical system, computation and modeling are powerful complements in several respects. Modeling and simulation are increasingly being seen as valuable guides to experimental efforts, as modeling studies have led to a better understanding of intracellular dynamics as well as tissue-level

phenomena. Simulation yields easily reproducible results, a great boon particularly in a biological field. The study of arrhythmias in the form of re-entrant electrical waves benefits greatly from the use of modeling and simulation because such results can provide insights otherwise unattainable solely through experimentation [1, 27, 2, 21, 9, 32, 17, 19]. Experimentally, many features of interest cannot be observed such as wave behavior within the interior of the muscle, but in simulation every aspect of the model is available for inspection and review.

While modeling efforts have produced many valuable insights regarding cardiac arrhythmias in general, comparably fewer studies have investigated the role of the Purkinje network during ventricular arrhythmias. Such studies require the incorporation of a structural model of the Purkinje network, and at present physical and experimental limitations make the retrieval of the physical Purkinje network structure impossible. Most studies that have modeled the Purkinje network structure have therefore constructed artificial Purkinje networks that are often either hand-drawn or in some cases generated algorithmically based on fractal-like branching structures. These artificial networks are often incorporated into ventricular models with the goal of reproducing normal activation times and sequences to match experimental observations.

A key feature of the development of current Purkinje structural models is that their construction is designed or guided by the modeler. One methodology that would avoid this shortcoming is to base Purkinje structural models directly on anatomical data; unfortunately, it is not currently possible to capture the intact three-dimensional Purkinje network structure. One recent study has attempted to overcome this limitation by making use of imaging data of the Purkinje network in the form of photographs. In 2012 Cherry and Fenton made use of the fact that the Purkinje network can be revealed through dissection of the ventricles to obtain two-dimensional photographs of the network structure [7]. In their work, they used these photographs to create two-dimensional Purkinje structural models and created a model of the combined ventricle-Purkinje system. Their work was the first instance of a Purkinje structural model based directly on anatomical data.

The goal of this thesis is to extend this recent approach to accurately model and incorporate the three-dimensional Purkinje structure into an anatomically realistic model of the ventricles. The development of these models for the ventricular system will form a basis for the further study of ventricular arrhythmias and the effect the Purkinje network has on arrhythmia dynamics in the ventricles.

The remainder of this thesis is arranged as follows. In Section 2 we present an overview of cardiac

physiology and anatomy, as well as the typical modeling strategies used, with a focus on those methods we use in our work. In Section 3 we discuss what work has been done in the area of modeling the Purkinje network. In Section 4 we present the method we developed by which digital photographs of Purkinje networks used in conjunction with ventricular anatomical data can be used to reconstruct and map the Purkinje network onto the ventricular endocardial surfaces – what we will refer to as the texture-mapping problem. In Section 5 we present two novel approaches for modeling what we term coupled ventricle-Purkinje systems. Finally, in Section 6 we discuss results, including implications and limitations, and then suggest several avenues for future work.

2 Overview of Cardiac Anatomy and Models

2.1 Cardiac Tissue as an Excitable Medium

In investigating cardiac arrhythmias, we study cardiac cells and tissue as an excitable medium. Excitable media are characterized by several important properties: a stable rest state, a stimulus threshold, excitability, refractoriness, wave propagation without damping, and the support of spiral and scroll waves [16].

A cardiac cell is an excitable medium. Its stable rest state is characterized by the cell membrane potential settling to a resting value of around -80 mV, along with there being no net transport of ions across the cell membrane. A cardiac cell has a stimulus threshold of around -60 mV [22]; stimuli that cause the membrane potential to rise above this level will cause the cell to excite. The form an excitation takes on in cardiac cells is that of the cardiac action potential (other types of cells can have slightly different characterizations): an abrupt depolarization of the cell membrane potential from its resting potential followed by a much more gradual repolarization back to the resting potential. Cardiac cells are refractory in that after generating an action potential, they cannot generate any further responses to stimuli for some time; in essence, the cell must recover after generating a response.

Cardiac tissue is composed of many cardiac cells coupled electrically in a diffusive manner. Physiologically, the mechanism behind the coupling of cells is gap junctions – specialized structures that connect cells [28]. Through this coupling, action potentials generated in a cell can induce action potentials in neighbor cells. This coupling results in the support of waves of depolarization that spread throughout tissue; exciting a small patch of cardiac tissue will result in an outward-propagating wavefront that does not damp out over time.

Incorporating spatial dimensions into excitable media allows for complex patterns to emerge. In two dimensions a type of re-entrant wave called a spiral wave [16] can occur, in which a wave front rotates around a point: the spiral tip. These waves can exist in a stable state in which they never terminate, or they may eventually break up into many smaller re-entrant waves. In two-dimensional tissue, the wave front can be thought of as one-dimensional and rotating around a zero-dimensional point; in three dimensions, a wave front then is two-dimensional, and a re-entrant wave consists of such a front rotating around a one-dimensional spiral filament. Typically these

complex phenomena involving re-entrant waves do not subside naturally. In patients, such electrical behavior in the heart results in various cardiac arrhythmias. A single re-entrant wave is often the cause of tachycardia, a type of arrhythmia in which many rapid heartbeats are registered. This can often transition into the more serious condition of ventricular fibrillation, which is caused by the emergence of several re-entrant waves, typically after a single re-entrant wave 'breaks' into multiple waves. In these cases, the patient typically must be subjected to defibrillation, in which electrodes are used to force all tissue in the heart to depolarize or repolarize, thereby 'resetting' the tissue in order to disrupt the re-entrant waves.

2.2 Cardiac Cell Models

Cardiac cell dynamics are often modeled with systems of ordinary differential equations [12, 15]. Such models may either be phenomenological or function by modeling intracellular dynamics. These latter models are referred to as ionic models because they model the membrane potential by tracking various transmembrane ion currents [12]. The equations of such systems are typically highly nonlinear and the number of variables in the systems varies greatly among models. There are popular two- and three-variable models [23, 20, 13] as well as much more complex and detailed models with dozens of variables [12, 15]. Smaller models are well-suited for studying tissue-level phenomena such as spiral- and scroll-wave dynamics, whereas more complex models are more often used in the study of cellular dynamics. Regardless of the level of detail or sophistication of these models, they most commonly can be expressed in the form

$$\frac{dV}{dt} = -\frac{I_{ion}}{C_m}, \tag{1}$$

where V is the membrane potential of the cell, C_m is the membrane capacitance of the cell, and I_{ion} is the sum of various transmembrane currents, usually governed by several other time-dependent variables. Thus (1) actually is one of a system of equations that in some models can be highly complex. Other model equations can be summarized by

$$\frac{d\vec{y}}{dt} = f(\vec{y}, V, t),$$

where $\vec{y}$ is a vector referring to the various model variables. These model variables are typically ionic current gating variables or intracellular ion concentrations [12].

In the absence of stimuli, the cell will maintain a stable rest state; initial conditions for these models are typically given by modelers to be values at or near this state.

2.3 Modeling Cardiac Tissue

Cardiac tissue is often modeled as a continuum of cardiac cells [8]. In this manner, the cardiac cell equation (1) can be transformed into a reaction-diffusion equation, where an ionic model for cardiac cells governs the reaction and the membrane potential is allowed to diffuse spatially according to the Laplacian. In this way, an ODE model for cardiac cells can be turned into a PDE for cardiac tissue, as in (2).

$$\frac{\partial V}{\partial t} = -\frac{I_{ion}}{C_m} + D\Delta V \tag{2}$$

Here D is the diffusivity of the membrane potential. Typically, no-flux or periodic boundary conditions are also imposed when using such a model.

Tissue-level simulations can be as simple as solving the cardiac reaction-diffusion equations on one-dimensional cables or on rectangular domains. In these simulations, many phenomena of interest to the study of cardiac arrhythmias can appear, such as spatially concordant and discordant electrical alternans, spiral waves, and wave break.

The physical structure of the domain on which the cardiac reaction-diffusion equations are solved can have a significant affect on the various arrhythmic phenomena that the tissue can support. One canonical example is that of an annulus-shaped tissue; in such a domain, the tissue itself supports a type of re-entrant wave in which the wave front propagates around the ring continuously. Such anatomically-supported re-entrant waves are referred to as anatomical re-entrant, whereas a spiral wave revolving around a spiral tip is referred to as functionally re-entrant. While similar behavior can occur in rectangular domains in the form of a spiral wave, such a wave will have a spiral tip around which it revolves, whereas in the case of the annular domain, the central void functions as an anatomical feature that 'pins' the reentrant wave.

2.4 Whole-Heart and Ventricle Simulations

Moving to tissue or whole-heart simulations often necessitates the inclusion of another cardiac feature to capture tissue-level phenomena accurately: fiber orientation. So far in our discussion we have assumed that spatial diffusion of the membrane potential is isotropic, though in reality this is not the case. Cardiac tissue is a muscle composed of fibers with an associated direction or orientation. The effect of these fibers is that the membrane potential diffuses more rapidly in

the direction parallel to the fibers and more slowly perpendicular to the fiber direction [28]. A typical ratio of the parallel and perpendicular diffusivities is 5 : 1 to 10 : 1 [14, 8]. The physical reason for this is the density of gap junctions is greater at the ends of the cells, relative to the fiber orientation. To account for this, the cardiac reaction-diffusion equations (2) can be modified [13] by the introduction of a local fiber orientation tensor $\mathbf{D}(x)$.

$$\frac{\partial V}{\partial t} = -\frac{I_{ion}}{C_m} + \nabla \cdot \Big(\mathbf{D}(x) \nabla V \Big) \tag{3}$$

Whereas previously in (2) the parameter D was a scalar, here $\mathbf{D}(x)$ is a tensor defined over the domain of interest, that accounts for the increased conductivity in the direction of the fibers.

The heart is composed of many layers of muscle that lie in varying orientations; the variety in fiber orientation makes the uniform contraction of the cardiac muscle possible. It is commonly regarded that these layers are parallel to the inner and outer surfaces of the heart, so the fiber direction of each layer lies primarily in this plane. Fibers typically follow approximate geodesic lines as they wind their way around the heart [26]. Moving from the endocardium to the epicardium, the fiber orientation within each layer changes [30, 24]. In reality, the distinction of there being discrete layers is made more for illustrative purposes; the layers in fact form a continuum, with the fiber orientation changing smoothly between some angle θ_i with respect to the axis normal to the cardiac surface at the endocardium and some angle θ_f at the epicardium.

Whole-heart simulations provide useful information about how the anatomical structure of the heart can affect arrhythmia dynamics. Such simulations consist of solving the cardiac reaction-diffusion equations on anatomically-realistic domains, recovered experimentally from real hearts. Anatomical data sets can be obtained through several means, such as dissection [24, 29] or image segmentation of MRI scans of an intact heart [3]. The means by which such models are implemented computationally are most often finite differences or finite elements. Finite-element methods naturally support domains of arbitrary structure, most often specified by a triangulated mesh surface or volume. Implementations utilizing finite differences require additional tools to implement arbitrary domains, such as in the work by Fenton et al. in which the phase-field method was used [14], or variations such as that of Buzzard et al. [5]. In our work we utilize a finite-difference scheme, and a more in-depth discussion of the topic can be found in Section 5.

Ventricular simulations generally omit the atria from the cardiac structure to focus solely on the electrical activity of the lower chambers of the heart. The atria and ventricles are nearly completely

electrically insulated from one another, making the study of the ventricles in isolation a reasonable simplification.

2.5 Cardiac Anatomy and Normal Heart Rhythm

The heart is composed of four chambers: two atria and two ventricles. The atria act to receive blood and are significantly smaller than the ventricles, which fill with blood from the atria and then expel it from the heart through contraction. When the heart is functioning healthily and normally, it is undergoing normal heart rhythm. Normal heart rhythm consists of several events, the timing of which is important to produce an effective contraction to pump blood. We have so far in our discussion focused mainly on the electrophysiological properties of cardiac cells and tissue rather than mechanical or contractile properties. Though contraction of the heart can have some effect on the electrical activity of the heart, this effect is usually minimal. Conversely, the mechanical contraction of cardiac tissue is a response usually directly related to the electrical activity. The timing of electrical events is thus important to produce muscle contraction, and disorganized electrical activity amounts to disorganized contraction.

From an electrical standpoint, a 'heartbeat' begins with the sinoatrial node. The sinoatrial node is a cluster of specialized pacemaker cells, meaning that they are auto-oscillatory rather than just excitable: they spontaneously generate action potentials. The sinoatrial node initiates heartbeats by generating action potentials that spread throughout the atria in a diffuse manner. This causes the atria to contract, causing blood to enter the ventricles. Located near the electrical boundary between the atria and ventricles is another cluster of specialized cells called the atrioventricular node, which is positioned such that it is activated after most of the atrial tissue has depolarized. The atrioventricular node in turn stimulates the Bundle of His, a collection of long bundles of fibers. The His bundle transitions and splits into the left and right Purkinje network branches, which are structures composed of another type of cell called Purkinje cells. Purkinje cells are specialized in that they conduct action potentials much more rapidly than normal cardiac tissue. The left and right Purkinje network branches are tree-like structures that have fine detail and span much of the interior to mid-layer volume of the ventricles. Each Purkinje branch serves to disperse a stimulus throughout the entire ventricles by stimulating the endocardial surface, which then spreads to the surrounding ventricular tissue. In this way, all tissue in each ventricle is depolarized fairly quickly, causing the ventricles to contract and pump blood out of the heart in a manner more effective than

normal repolarization would facilitate.

2.6 The Purkinje Network

The Purkinje network has a vital role in normal heart rhythm. While the atria have a somewhat less complicated role than the ventricles of passively filling with blood, the ventricle serve to pump blood out of the heart and throughout the body through contraction. The Purkinje network is necessary to quickly initiate coordinated depolarization across each ventricle because of the large musculature of the ventricles, the relatively slow conduction velocity of normal cardiac tissue (about a fourth of the conduction velocity of Purkinje fibers), the activation sequence needed in the ventricles to produce an effective contraction, and the timescale on which excitation must occur.

The placement of the Purkinje network is important to its function, as a modeling concern and for physiological reasons. In all species, the Purkinje network lies on the endocardium or just beneath the endocardium within a sub-endocardial layer. In many species (such as canines and humans, with a notable exception being ungulate species), the Purkinje network is almost entirely superficial to the endocardial surface. Thus when the ventricles are activated by the Purkinje network they are first activated at sites located at the endocardium and later at the epicardium as the wave of depolarization spreads outward. Figure 1 shows isochrone plots of typical activation times of the human heart, taken from the work of Durrer et al. [11]. Due to the Purkinje network, activation begins at the endocardium.

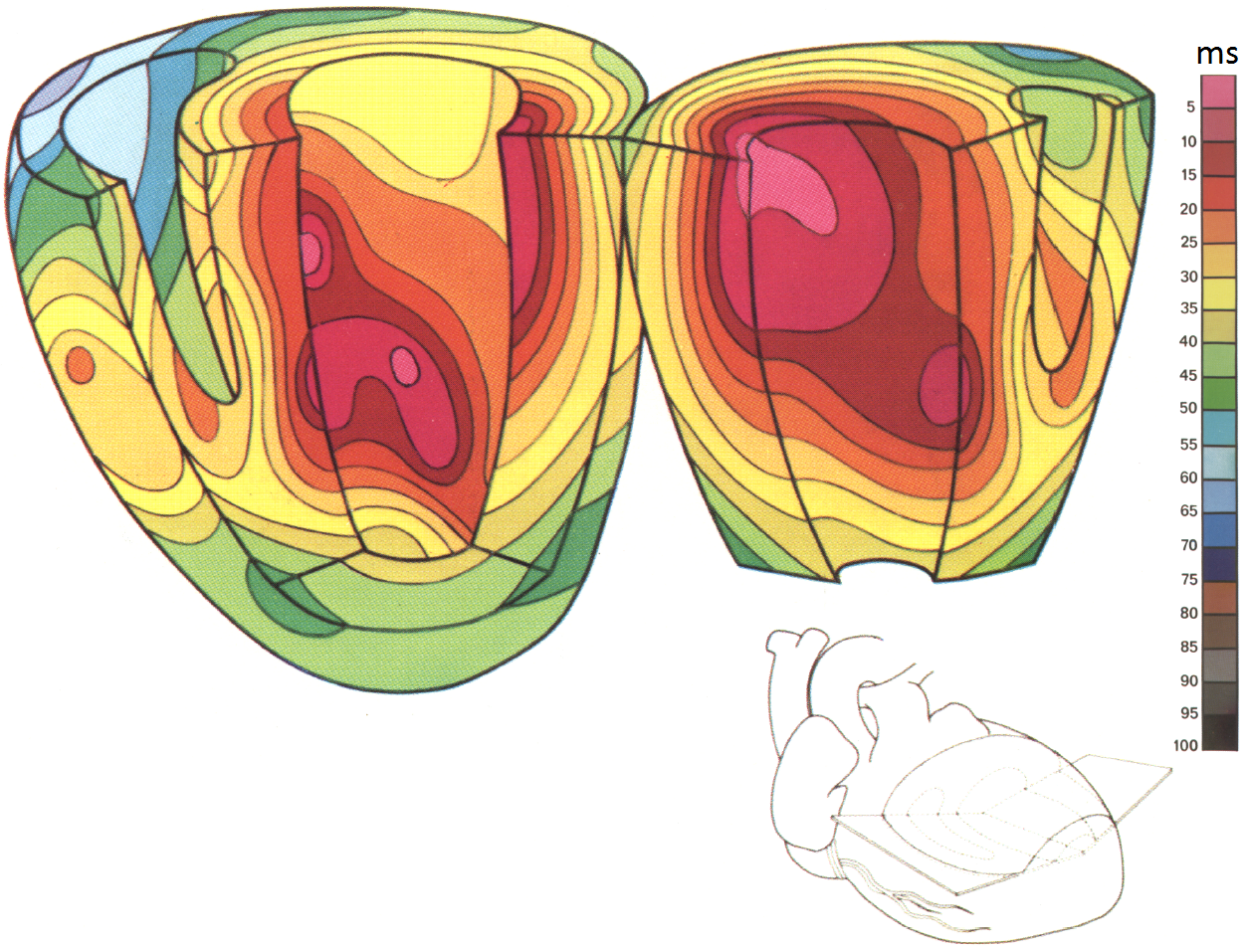

Figure 1: Activation sequence of the human heart. Plots show isochronal maps of the activation time of the tissue at each point. The heart is shown in a split view with the main segment in an anterior orientation. Activation begins primarily from the left endocardial surface, and the right ventricular free wall is the last region to be activated. Modified from Ref. [11].

3 Research Aim and Prior Work

3.1 Prior Work

As discussed in Section 1, the Purkinje network is crucial to normal heart rhythm. The effect of the Purkinje network during ventricular arrhythmias is much less well understood. Experimentally, evidence suggests that the Purkinje network may play a significant role in ventricular fibrillation. In 1995, Janse et al. compromised the Purkinje network in pig ventricles by cryoablating the endocardium and found that ventricular fibrillation could no longer be initiated [18]. In 2008, Dosdall et al. produced similar results after chemically ablating the Purkinje network in canine hearts: ventricular fibrillation terminated more quickly [10]. Many modeling efforts have been made to incorporate Purkinje-like networks into ventricular models. Though many methodologies have been employed in the creation of these networks, common to almost all modeling efforts so far is that the Purkinje network is manually or artificially generated rather than being based on anatomical data.

In several studies, relatively simple Purkinje networks have been constructed to mimic known anatomical features of the Purkinje network, such as its position and coverage of the endocardial surfaces. In 1998 Berenfield and Jalife created a Purkinje structural model by a procedure in which a manually drawn Purkinje network was projected onto the endocardial surface by "laying it onto the detected endocardial surfaces" [2]. The exact procedure by which this was accomplished was not detailed extensively, nor was it the focus of their work; rather, their goal was the creation of a structure having Purkinje-like characteristics, such as extent and area of the endocardial surfaces covered by the network. Clements and Vigmond developed a procedure by which a ventricular anatomical structure in the form of a triangulated mesh could be used to develop a Purkinje structural model [9, 32]. Their method began by first isolating the portion of the model mesh constituting the endocardial surfaces. A sophisticated flattening algorithm then was used to map the triangles in the endocardial meshes to the plane. Next, a manually drawn Purkinje network was laid onto the endocardial surfaces and the flattening transformation was inverted, yielding a three-dimensional Purkinje structure compatible with the initial cardiac structure.

Some studies have focused on modeling the Purkinje network structure for the purpose of reproducing experimental observations regarding the normal activation sequence of the heart. In 1998 Siregar et al. constructed a model for the combined ventricles-Purkinje system, in which the Purk-

inje network was generated to primarily activate regions of the ventricles observed experimentally to be sites of first activation [27]. Simelius et al. used a similar approach to design a model of the ventricular system that produced activations consistent with observed activation sequences and timings of the human heart, as well as with ECG data [21]. In 2008, Tusscher and Panfilov created a ventricular model incorporating a conduction system to investigate the role of the Purkinje network in normal and abnormal conduction [19]. Their approach to generating a Purkinje network relied on user-specified terminal Purkinje fiber sites, which were then used to generate the full network.

Some work has done in constructing Purkinje-like networks by generating branching structures based on fractal-like patterns. In 1991, Abboud et al. modeled the Purkinje network for use in reproducing ECG data through simulation [1]. In their work, the Purkinje network was modeled as a self-similar branching tree structure, in which the initial His bundle connection of the network divided symmetrically into two smaller branches, which each further divided into smaller branches. In 2008, Ijiri et al. developed an algorithm based on the L-system for generating Purkinje networks given a cardiac structure [17] and limited user input. The L-system is a formal grammar that can implement a system for generating fractal-like structures based on simple rules, originally developed for modeling plant cells and structures. In their work, Ijiri et al. used the L-system to generate a branching mesh structure that was confined to the endocardial surface starting from a number of user-defined 'terminal locations'.

All of the methods for constructing Purkinje networks so far discussed have used either hand-drawn or computer-generated networks based on general principles. Very little work has been done on using experimental data to directly create Purkinje structures. The reason for this is most probably technological limitations: MRI and other means by which three-dimensional structures may be isolated cannot be applied to capture the Purkinje structure because there is little to no difference in Purkinje muscle density as compared to the surrounding cardiac tissue.

One avenue for combating this limitation takes advantage of the placement of the Purkinje network. The confinement of the Purkinje network to the surface of the epicardium makes the experimental observation of the network possible. Though normally indistinguishable from surrounding cardiac tissue, Purkinje fibers, when treated with Lugol's solution, stain darker. Experimentally, this allows for two-dimensional images of the macroscopic network structure to be photographed from dissected ventricles. In 2012 Cherry and Fenton utilized photographs obtained in this manner to create a

digitized Purkinje structure for use in a ventricle-Purkinje simulation [7].

Cherry and Fenton's ventricle-Purkinje model was the first structural model of the Purkinje network based directly on experimental data. Their work showed that the integration of a Purkinje network into simulations of cardiac tissue can lead to significant differences in arrhythmia dynamics. Their work integrated a Purkinje network into a cylindrical cardiac tissue and found that spiral wave dynamics were altered in both their genesis as well as maintenance. In their work, Cherry et al. used the phase-field method to solve the system on a complex tree-like domain recovered from a digital photograph of a Purkinje network obtained through dissection. The Cherry-Fenton ventricle-Purkinje model was limited in that it lacked a realistic ventricle anatomical structure and only modeled one ventricle and associated Purkinje branch. Nevertheless, this was the first work in which imaging data taken directly from experiments was used to create a structural model of the Purkinje network.

3.2 Research Aim

The goal of this thesis is the development of a model and modeling techniques for the combined ventricle-Purkinje system to form a basis for the study of ventricular arrhythmias. In contrast with existing work in the field, we seek to model the Purkinje structure through the direct use of imaging data taken from experimental photographs.

Our modeling approach is to couple a ventricular model and a compatible Purkinje model. Since it currently is impossible to directly recover the physical three-dimensional Purkinje structure, our first step is the development of a method for reconstructing this structure from photographs and anatomical data. We then use this method to create the Purkinje structural models, implement the Purkinje and ventricular models, and then couple them to produce a model for the entire ventricular system.

An accurate model of the ventricle-Purkinje system will reproduce important features of the normal activation sequence of the ventricles. Specifically, the time and sequence by which points in the ventricles are depolarized is fairly well-known. The goals we pursue in the development of our models is to achieve full activation of ventricles through a stimulus delivered by the Purkinje network, and to chronologically activate the same regions within the ventricles as observed experimentally within the correct amount of time.

3.3 Materials

3.3.1 Digitized Purkinje Network

The digital Purkinje structures used in our work were extracted from photographs obtained through experiments done by colleagues. Researcher Flavio Fenton obtained photographs of the canine Purkinje network through a procedure in which the ventricles were dissected and treated with Lugol's solution, which preferentially stains Purkinje fibers darker than the surrounding cardiac muscle. The experiment was performed on multiple ventricles; in our work we use Purkinje networks recovered from a left and right canine ventricle. Figure 2A shows the left ventricle photograph, and Figure 3A shows the right ventricle photograph.

Following the collection of the photographs, the networks were digitized manually by tracing the darkened fibers in an image-editing program. The left ventricle Purkinje network digitization used in our work is the same as that used in Cherry and Fenton's work [7]. The right ventricle Purkinje network was digitized as part of the work of this thesis. Due to the dissection method of the right ventricle, network connections were severed, and we did not make any efforts to match severed fibers across the dissection incision.

Figures 2B and 3B show the digitized Purkinje networks overlaid onto the experimental photographs from which they were extracted, and Figures 2C and 3C show the isolated digitized Purkinje networks. Coupling sites were next added at the apparent end of each Purkinje fiber. The left ventricle network had a total of 130 coupling sites and the right network had 100 coupling sites.

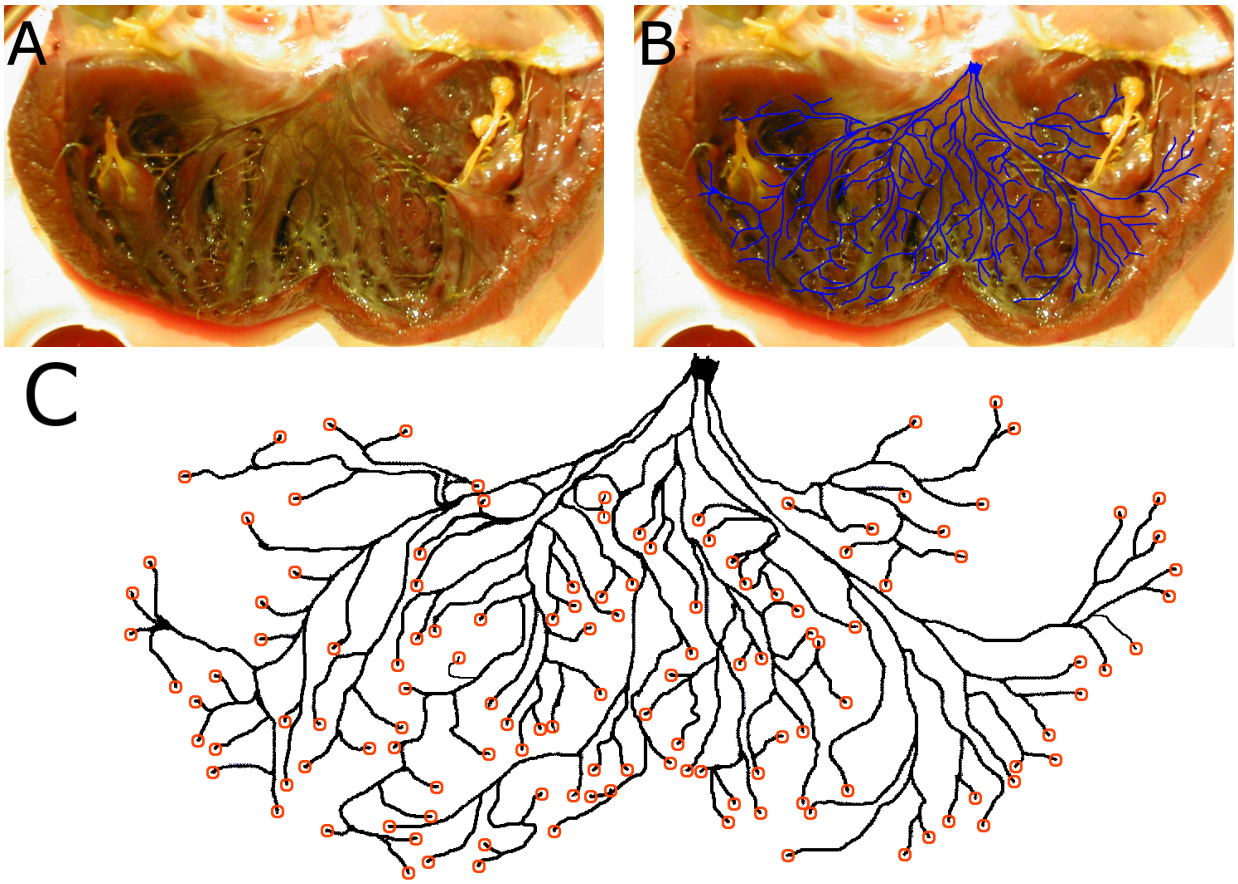

Figure 2: Digitization of the canine left ventricular Purkinje network. (**A**) Photograph from experiment in which the left ventricle was dissected and treated with Lugol's solution, staining the Purkinje network darker than surrounding tissue. The Purkinje network is visible to the eye. The left bundle branch is visible in the center at the top of the photograph, which corresponds to the septum wall. (**B**) Visible Purkinje fibers are manually traced in an image-editing program; the resulting network structure is overlaid for comparison onto the photograph from which it was extracted. (**C**) The resulting digitized Purkinje structure. Coupling sites – located at the ends of the fibers – are indicated by orange circles.

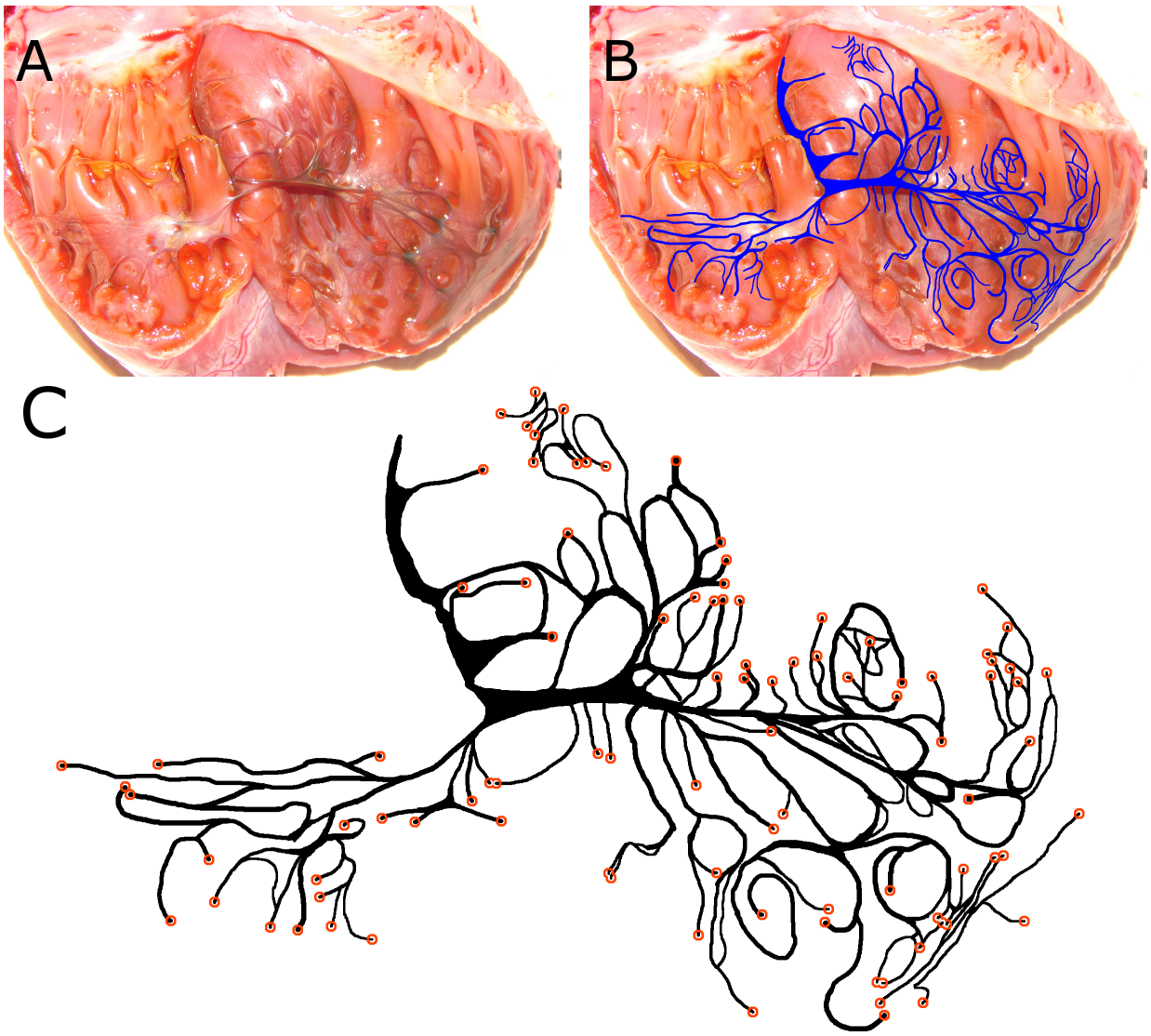

Figure 3: Digitization of the canine right ventricular Purkinje network. (**A**) Experimental photograph in which the left ventricle was dissected and treated with Lugol's solution, staining the Purkinje network darker than surrounding tissue. The Purkinje network is visible to the eye. The dissection method here involved a cut along the 'seam' between the septum and free wall; the septum is positioned on the left and the free wall on the right. Non-Purkinje fibrous tissue can be seen in the upper left corner of the photo; this tissue attaches to valves and is not part of the Purkinje network structure. (**B**) Visible Purkinje fibers are manually traced in an image-editing program; the resulting network structure is overlaid for comparison onto the photograph from which it was extracted. (**C**) The resulting digitized Purkinje structure. Coupling sites – located at the ends of the fibers – are indicated by orange circles.

3.3.2 Ventricle Structures

In our work we utilized both a canine and a rabbit ventricular anatomical structure.

Canine Ventricular Structure The canine ventricular structure that we worked with was recovered in 1991 by Nielsen et al.[24]. The ventricles are embedded in a rectangular regularly-spaced numerical grid of size $400 \times 320 \times 320$ with $\Delta x = 0.025$cm. Figure 4 shows various isosurface plots of the canine ventricular data set.

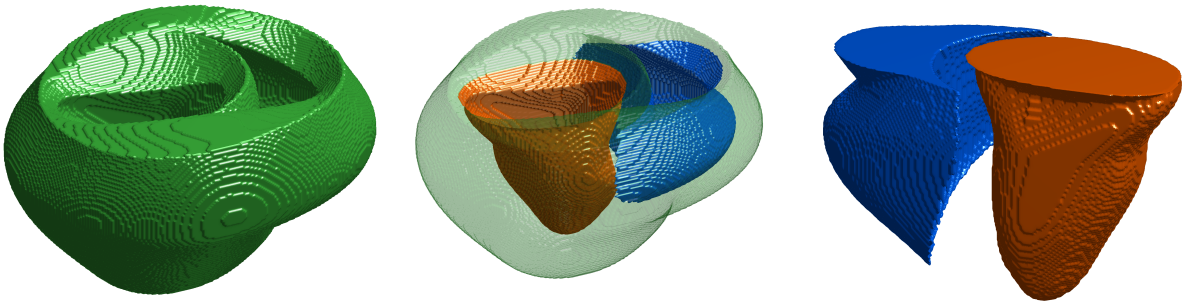

Figure 4: Isosurfaces of the canine ventricular structure used in our work. (**Left**) The entire ventricular structure in a posterior viewing orientation. (**Center**) Transparent overlay of the epicardial surface in line with the endocardial surfaces, shown for comparison and orientation. The left endocardial surface is shown in orange and the right endocardial surface is shown in blue. (**Right**) Alternate viewing angle of the isolated endocardial surfaces of the left and right ventricles.

Rabbit Ventricle Structure The rabbit ventricles structure that we worked with was obtained in 1998 by Vetter and McCulloch [31]. The ventricles are embedded in a rectangular regularly-spaced numerical grid of size $138 \times 130 \times 152$ with $\Delta x = 0.025$cm. Figure 4 shows various isosurface plots of the rabbit ventricular data set.

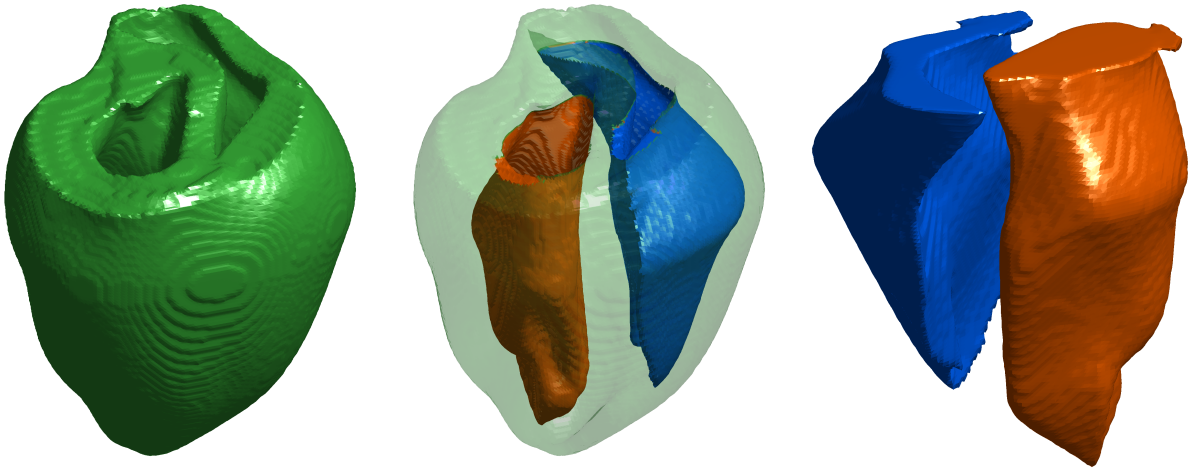

Figure 5: Isosurfaces of the rabbit ventricular structure used in our work. (**Left**) The entire ventricular structure in a posterior viewing orientation. (**Center**) Transparent overlay of the epicardial surface in line with the endocardial surfaces, shown for comparison and orientation. The left endocardial surface is shown in orange and the right endocardial surface is shown in blue. (**Right**) Alternate viewing angle of the isolated endocardial surfaces of the left and right ventricles.

4 Texture Mapping

The development of a model for the ventricle-Purkinje system requires a structural model of the Purkinje network. Previous attempts in modeling the three-dimensional Purkinje network structure have made use of artificially generated networks [1, 27, 2, 21, 9, 32, 17, 19]. In our work, we aim to develop Purkinje structural models based directly on imaging data of real Purkinje networks taken from experimental dissections. Imaging data in the form of photographs can be used to digitize the two-dimensional structure of the Purkinje network, but such data cannot be used directly to model the three-dimensional Purkinje structure. Here we present a technique we have developed for projecting the two-dimensional Purkinje structure onto the endocardial surfaces of ventricular data sets. Due to similarities between this task and that of standard texture-mapping, we term this problem the texture-mapping problem.

Though texture-mapping is a well-known procedure, the problem of interest here is not a typical texture-mapping problem. In standard texture mapping, an image (typically referred to as the texture image) is applied to a polygon mesh model so that for each face of the polygon model, some portion of the texture image is mapped to it in a manner that results in a smooth transition between faces. Here, we are neither working with a polygon model nor, strictly speaking, texturing a surface, but rather texturing a thin shell that nevertheless has width. The procedure we outline here projects the texture image to this shell, throughout its thickness.

In this section we first present a high-level overview of what we refer to as the texture-mapping problem. Next, we discuss the mathematical formalism involved in the procedure we developed to accomplish this goal, followed by an overview of several key points regarding the method, including implementation concerns. Finally, we present results in which three-dimensional Purkinje networks are constructed through our method, by projecting digitized Purkinje networks onto ventricular endocardial surfaces.

4.1 Overview

Our strategy consists of two steps. First, map the texture image onto some surface that approximates the target surface. Second, perform a procedure to map from the approximating surface to the target surface. In our work, the texture image is derived from a digital photograph of a Purkinje network, and the target surface is a ventricular endocardial surface.

When we say that our goal is to texture-map a surface, this is not entirely accurate for two reasons. First, generally texture-mapping refers to mapping a texture image onto a surface composed of polygons - a polygon mesh. In our context, the surface or data that we wish to texture-map is more comparable to a voxel model; the surface is implicit in the data set with which we are working rather than specified explicitly. Second, our goal is to texture-map a relatively thin shell rather than a surface that has no thickness. Later we will solve reaction-diffusion equations using finite-difference methods, and the grid spacing used in those methods must be smaller than the thickness of this shell. The reason for this is our use of the phase-field method for solving these systems on arbitrary domains - the phase-field method can only represent domains with detail coarser than the space-step of the solution grid.

We use right-cylinders as our approximating surfaces. The left and right ventricular endocardial surfaces both have vertical cross-sections that are fairly consistently aligned with the vertical axis, making their approximation by cylinders appropriate. The anatomical morphology of the endocardial surfaces as well as their orientation in the data sets we used lend themselves quite well to cylindrical approximations.

There are several advantages to using a cylindrical approximation as opposed to any arbitrary surface. First, the technique that we have developed involves establishing a curvilinear coordinate system based on the approximating surface. Choosing a cylinder aligned with a coordinate axis rather than an arbitrary surface allows this coordinate system to be built up in two parts: first in two dimensions, and then extended to a third, in a manner similar to how cylindrical coordinates are an extension of polar coordinates. This is much simpler and less computationally expensive than using an arbitrary surface. Second, whereas using an approximating shape such as a sphere or most any other shape would require distortion of the texture image, a cylinder is simpler in that a flat image can be embedded along the cylinder surface without distorting any distances. Finally, assuming the surface is oriented appropriately, the axis of the cylinder and that of the target surface can be aligned, which greatly simplifies the problem by eliminating the need for any rotational transformations.

4.2 Method

Let $C : [0, L] \to \mathbb{R}^2$ be a curve parameterized by arc length, where L is the total length of the curve. If C is a closed curve that is oriented in the counter-clockwise direction then taking the space $C \times \mathbb{R}$, we obtain a surface – a cylinder with base C. It is this cylinder that, in the context of the texture-mapping problem, is selected to approximate the surface to be textured.

Define $\vec{N}(s)$, the outward-pointing unit normal vector to the curve C at $\vec{C}(s)$, by

$$\vec{N}(s) = \begin{bmatrix} 0 & 1 \\ -1 & 0 \end{bmatrix} \vec{C}\,'(s)$$

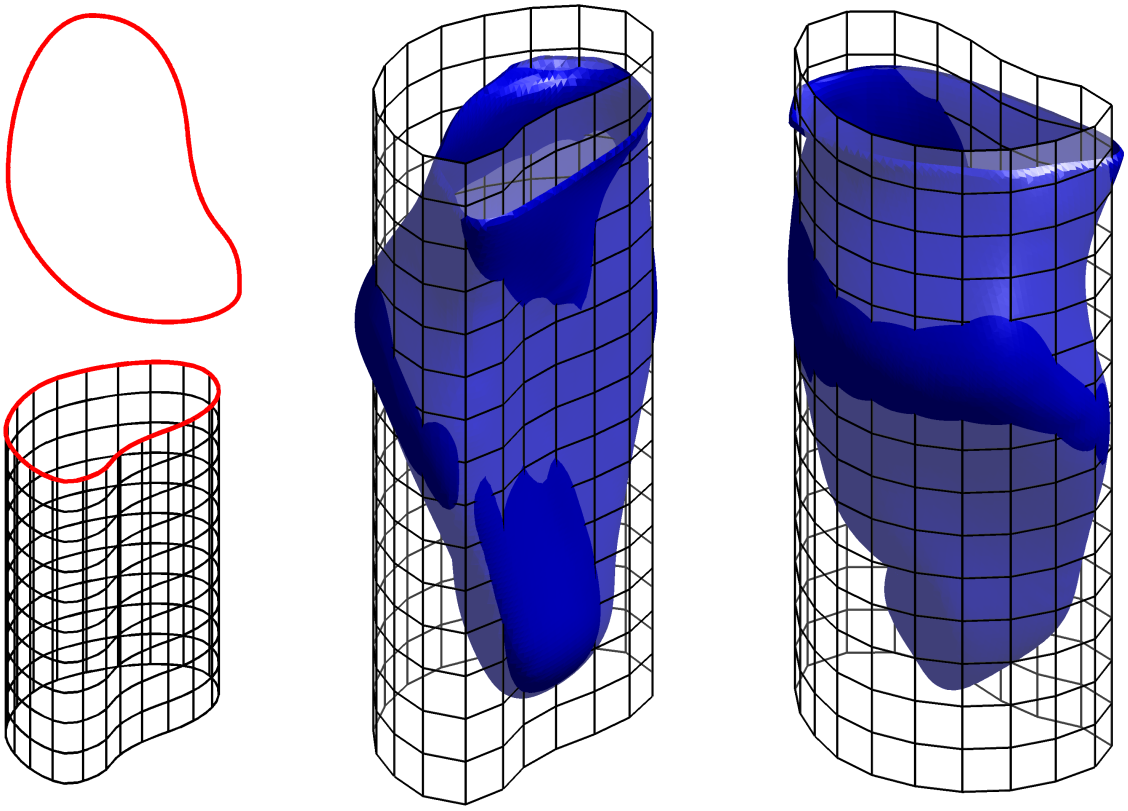

Figure 6: A choice of a curve C and the associated cylinder with base C. (**Left**) The curve in the plane is shown in red; the associated cylinder is shown in a different viewing angle. (**Center and Right**) The cylinder chosen to approximate an endocardial surface is shown aligned with the surface.

Define the vector field $\vec{V} : \mathbb{R}^2 \to \mathbb{R}^2$ by

$$\vec{V}(\vec{x}) = \frac{\int_0^L \vec{N}(s) d(\vec{x}, \vec{C}(s))^{-P} \, ds}{\int_0^L d(\vec{x}, \vec{C}(s))^{-P} \, ds}, \tag{4}$$

where d is the distance function and $P \geq 1$ is a constant. $\vec{V}(\vec{x})$ forms a weighted average of $\vec{N}(s)$ at every point along $\vec{C}(s)$, where the weights are given by the inverse of the distance from $\vec{C}(s)$ to the point p. As a consequence of this weighting scheme, we have that $\vec{V}(\widetilde{p}) \to \vec{N}(p)$ as $\widetilde{p} \to p$ for all $p \in C$; that is, $\vec{V}$ converges to $\vec{N}$ near points on C. The reason for this convergence is that at a point $\vec{C}(s_0)$ on the curve the two integrals in (4) diverge at s_0.

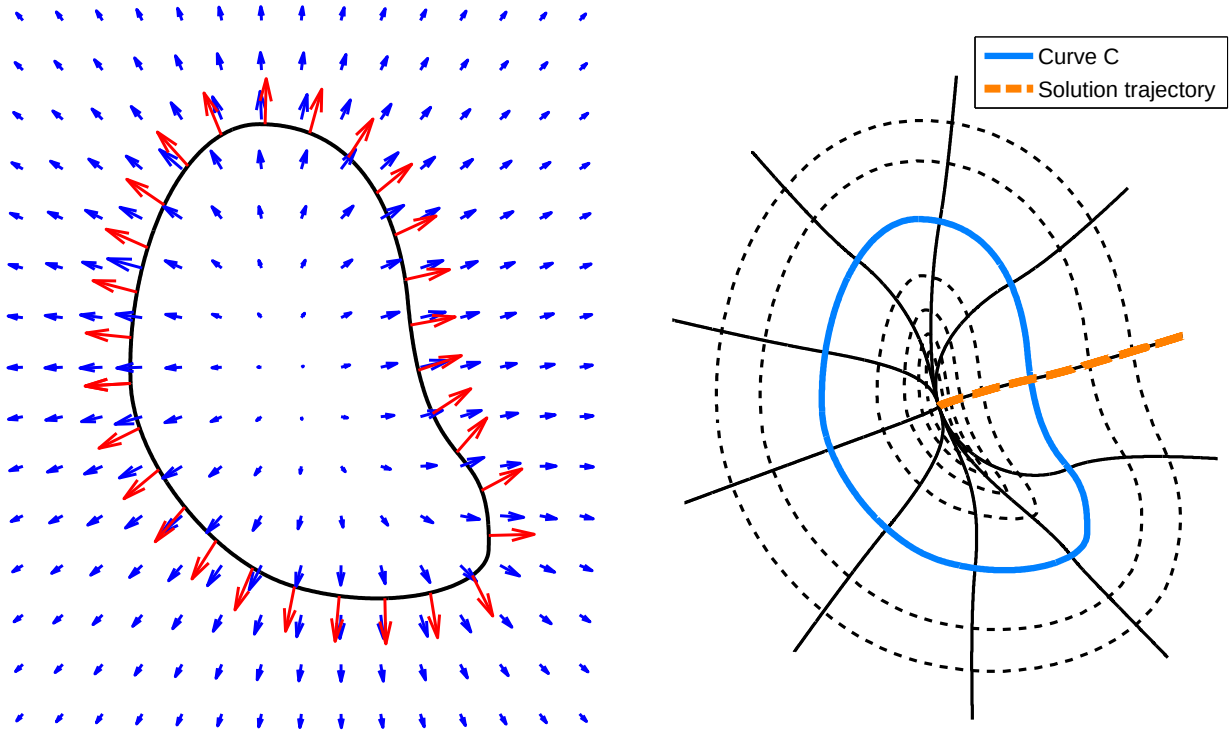

Figure 7: The vector field $\vec{V}$ and its solution trajectories. (**Left**) Shown in red is the outward-pointing unit normal vector $\vec{N}(s)$ to the curve C, shown in black. The blue vectors show a sampling of the vector field $\vec{V}$, defined everywhere. (**Right**) The curvilinear coordinate system resulting from taking solution trajectories to the vector field $\vec{V}$. Shown in blue is the original curve C; solid black lines (and the orange dashed curve) are solution trajectories representing lines of constant s in the coordinate system, and black dashed lines are lines of constant t. Note that where solution trajectories intersect C, they are orthogonal to C.

The system (5) is now of interest:

$$\frac{d\vec{x}}{dt} = \vec{V}(\vec{x}). \tag{5}$$

Here we introduce an artificial time parameter t for the purpose of obtaining solution trajectories of a particle moving through the vector field $\vec{V}$. In particular, for initial conditions $\vec{x}(0) = \vec{C}(s)$, we are interested in the solution $\vec{x}(t)$ for $-\infty < t < \infty$. Note that $\vec{x}(t)$ is normal to C at C because to the construction of V. We adopt the notation $(s,t)_C = \vec{x}_s(t)$, where $\vec{x}_s(t)$ is the solution to the initial-value problem given by (5) with initial condition $\vec{x}_s(0) = \vec{C}(s)$ for some $s \in [0, L)$, for $-\infty < t < \infty$.

For curves C of interest, taking the family of solutions to (5) establishes a curvilinear coordinate system, such that any point $(x, y) \in \mathbb{R}$ can be given by in curvilinear coordinates $(s,t)_C$ for some $s \in [0, L)$ and $t \in \mathbb{R}$. Note that $(s, 0)_C = \vec{C}(s)$.

We extend this curvilinear coordinate system in much the same way that cylindrical coordinates extend polar coordinates. Any point $(x, y, z) \in \mathbb{R}^3$ can be represented by $(x, y, z) = (s, t, z)_C$ for some $s \in [0, L), t \in \mathbb{R}$. Consider now the surface

$$\{(s, 0, z)_C : s \in [0, L), z \in \mathbb{R}\} \cong C \times \mathbb{R}.$$

This surface is the cylinder chosen to approximate the surface to be textured.

We now introduce the texture image that will be applied to the surface of interest. Let $T : [0, W] \times [0, H] \to \mathcal{P}$ be the texture image with width W and height H. Here $\mathcal{P}$ simply denotes the *palette* of which the texture image makes use. For a binary image we could simply have $\mathcal{P} = \{0, 1\}$, or an 8-bit RGB image could be represented by a palette $\mathcal{P} = [0, 255]^3$ for the red, green, and blue components of the colors of the image.

We next position the texture image on this cylinder. We select some subset $[a, b] \times [c, d] \subset [0, L] \times \mathbb{R}$, a rectangular portion of the cylinder in which the texture image will reside. If the aspect ratio of the texture image should be preserved, we ensure that $\frac{b-a}{d-c} = \frac{W}{H}$. A point $(s, 0, z)_C$ is assigned the texture value of the point (u_1, u_2), where

$$u_1 = W\left(\frac{s-a}{b-a}\right), \qquad u_2 = H\left(\frac{z-c}{d-c}\right).$$

That is, $T(u_1, u_2)$ is the texture value of the point $(s, 0, z)_C$.

This defines the texture value of a part of the cylinder. Using the curvilinear coordinate system we have established, we can extend this texture value definition along curves of constant s to define texture values for all points in $\mathbb{R}^3$. We now define an extension of our embedded two-dimensional texture image to three dimensions by constructing a function $F : \mathbb{R}^3 \to \mathcal{P}$.

$$F(x, y, z) = T(s, t, z)_C = T(s, 0, z)_C = F\left(W\left(\frac{s-a}{b-a}\right), H\left(\frac{z-c}{d-c}\right)\right)$$

4.3 Implementation Considerations

Defining the Curve C: Using Bezier Splines In our work, the curve C was chosen to be a closed Bezier spline – a piecewise-defined collection of third-degree Bezier curves. Bezier curves of degree three are parametrically defined curves of the form

$$B(t) = \vec{x}_1(1-t)^3 + 3\vec{x}_2(1-t)^2 t + 3\vec{x}_3(1-t)t^2 + \vec{x}_4 t^3,$$

where $\{\vec{x}_i\}_{i=1}^4$ are the control points of the curve. In general such a curve passes through the first and last control points only, with $B(0) = \vec{x}_1$ and $B(1) = \vec{x}_4$, whereas the other control points influence the path it takes when 'exiting' $\vec{x}_1$ and 'entering' $\vec{x}_4$ by determining the slope of the curve at the first and last control points.

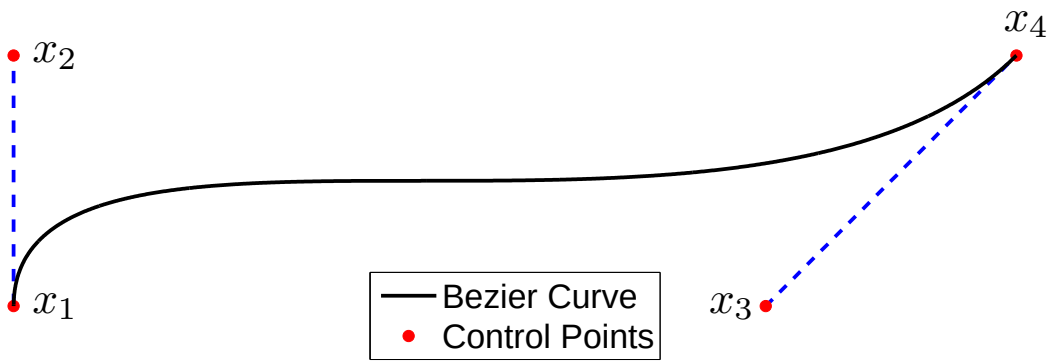

Figure 8: Schematic diagram of a Bezier Curve. The third-degree Bezier curve (black) is defined by four control points (red). The curve intersects the first and last control points, whereas the second and third define the slope at the first and last control points and control the overall shape of the curve.

A Bezier spline is a piecewise-defined function where each piece is a Bezier curve, chosen so that the first control point of a segment is the same as the last control point of the previous segment. In

our work, the Bezier spline and its component curves were always chosen to have continuous first derivatives. We generally used splines consisting of only five or six segments, which captured the key characteristics of the approximating cylinder for each ventricle surface satisfactorily.

Bezier curves in their natural parameterizations are not parameterized by arc length, which is an important requirement of the above outlined method. Fortunately, as opposed to reparameterizing the spline and its component curves, we can make an integral change of variable that yields equivalent results; details of this equivalency will be discussed momentarily.

Selecting the Curve C Choosing to define the approximating curve C using Bezier splines allows for a great deal of freedom in the selection of the curves. In our work, curves were selected by manual manipulation of the Bezier control points. To facilitate the easy selection of these curves, we built a graphical user interface in MATLAB that allowed for the configuration of Bezier splines. The program first took in a number of key control points through which the spline would pass, and then generated a closed spline plotted against its control points. At any time additional control points could be added (by splitting a spline segment into two sub-segments) where additional detail was required. The program allowed for the manipulation of the control points directly with the mouse, making fine-tuning the curves a simple procedure. The program also enforced colinearity of the control points associated with each end point of a spline segment, thus ensuring C^1 differentiability of the spline.

Defining the Vector Field V The definition of V given in (4) essentially interpolates the outward-pointing unit-normal vector at each point along the curve C. This definition was selected following our observations that a vector field based on interpolating the unit normal vectors along the curve yielded desirable properties; namely, that V is normal to C at C, and *near* C, and so solution trajectories passing through C are normal to C.

A Change of Variables to Simplify Expressions Most likely, a chosen curve will not be parameterized by arc length. Typically, this would mean that we should reparameterize the curve by arc length, but here we show a derivation for an alternative, equivalent approach.

Let $r : [a, b] \to \mathbb{R}^2$ be a curve not necessarily parameterized by arc length. Define the arc length

$s(t)$ and the outward-pointing normal (non-normalized) vector $N(t)$ by

$$s(t) = \int_a^t \left\|\vec{r}\,'(\tau)\right\| \, d\tau, \qquad\qquad N(t) = \begin{bmatrix} 0 & 1 \\ -1 & 0 \end{bmatrix} \vec{r}\,'(t),$$

$$V(\vec{p}) = \int_0^L \frac{\vec{N}(s^{-1}(\sigma))}{\|\vec{r}\,'(s^{-1}(\sigma))\|} d(\vec{p}, \vec{r}(s^{-1}(\sigma)))^{-P} \, d\sigma.$$

Now, $r\left(s^{-1}(\sigma)\right)$ is the arc length parameterized curve, and by change of variables, we have that for any function $G(t)$,

$$\int_0^L G\left(s^{-1}(\sigma)\right) \, d\sigma = \int_{s(a)}^{s(b)} G\left(s^{-1}(\sigma)\right) \, d\sigma = \int_a^b G(t) s'(t) \, dt.$$

In particular, consider the case where $G(t) = g(t)/\left\|r'(x)\right\|$. Here certain favorable cancellations occur since by the fundamental theorem of calculus, $s'(t) = \|r'(t)\|$, and so

$$\begin{aligned} V(\vec{x}) &= \int_0^L G\left(s^{-1}(\sigma)\right) \, d\sigma \\ &= \int_a^b \Big[G(t)\Big]\Big[s'(t)\Big] \, dt \\ &= \int_a^b \left[\frac{g(t)}{\|\vec{r}\,'(t)\|}\right] \Big[\left\|\vec{r}\,'(t)\right\|\Big] \, dt \\ &= \int_a^b g(t) \, dt. \end{aligned}$$

Here, if we take $g(t)$ to be, for some point $\vec{p}$,

$$g(t) = \vec{N}(t) d(\vec{p}, \vec{r}(t))^{-P} \, dt.$$

Then we have that

$$\vec{V}(\vec{x}) = \int_0^L \frac{\vec{N}\left(s^{-1}\sigma\right)}{\|\vec{r}\,'\left(s^{-1}(\sigma)\right)\|} d(\vec{x}, \vec{r}(s^{-1}(\sigma)))^{-P} \, d\sigma = \int_a^b \vec{N}(t) d(\vec{x}, \vec{r}(t))^{-P} \, dt.$$

Evaluating V Evaluating $\vec{V}(p)$ involves evaluating three line integrals along C and so is computationally expensive. In order to reduce the computational cost and runtime of the algorithm, we first evaluated $\vec{V}$ on a numerical grid of evenly spaced points. To evaluate $\vec{V}$ at any general point, we then interpolated this known grid of $\vec{V}$ values using the MATLAB function **interp2**.

The Parameter P In the definition of the vector field V in (4), we introduce the parameter $P \geq 1$. Though in our work we did not focus on the effects of varying P, it nevertheless has interesting effects on the vector field V and its solution trajectories and can be useful as a control parameter when attempting to texture-map a surface.

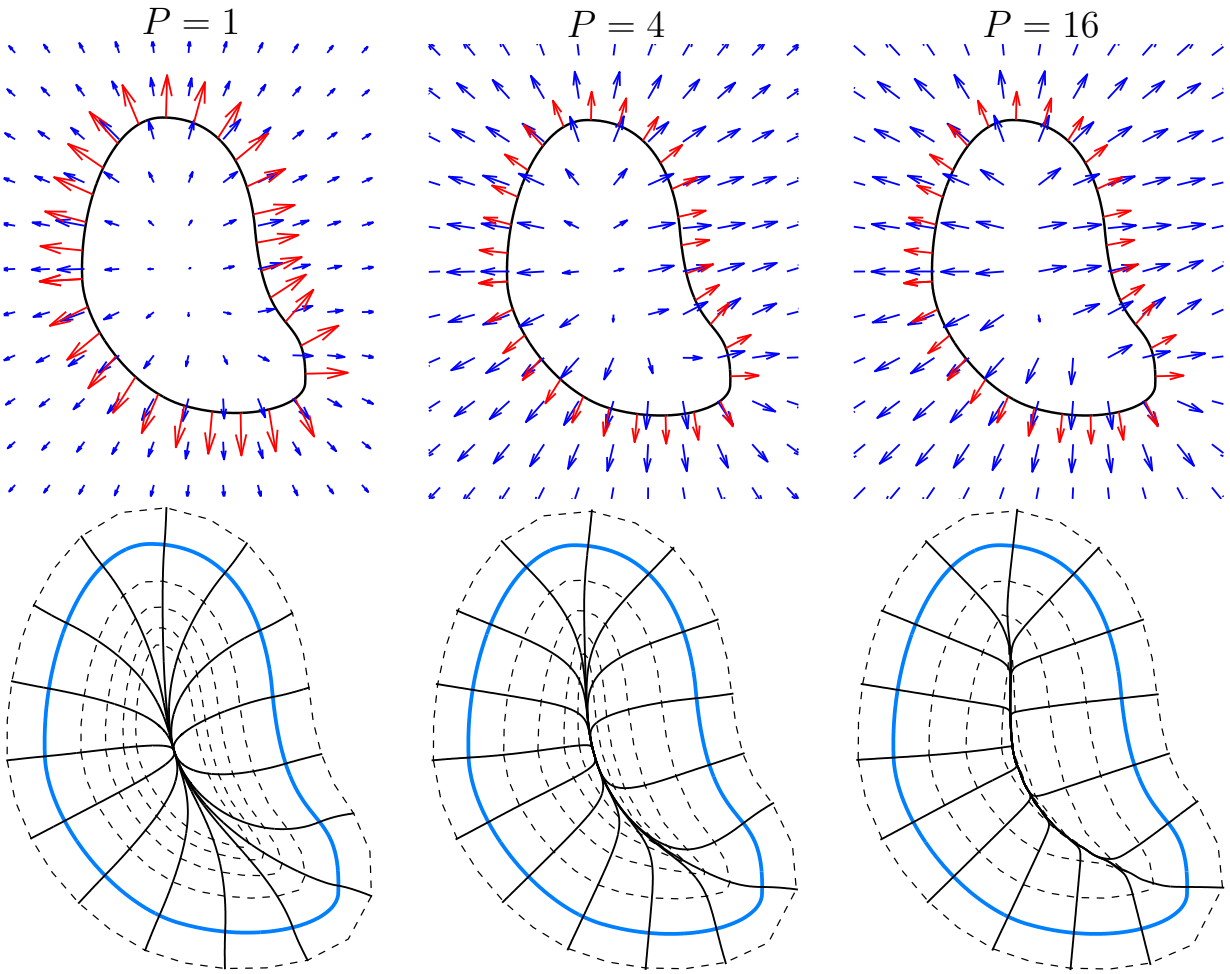

Figure 9: (**Top**) The vector field V for various values of P and (**Bottom**) associated induced curvilinear coordinate systems. Lower values of P result in 'smoother' trajectories that quickly deviate from the direction normal to the curve, whereas larger parameter values result in 'sharper' trajectories that follow more closely the direction normal to the curve.

When $P = 1$, the vector field V at a point $\vec{x}$ takes on a weighted average of the outward-pointing unit-normal vector to the curve C, where the weights are given by the reciprocal of the distance from $\vec{x}$ to every point on the curve. For other values of P, the weight is the reciprocal of the P-th power of this distance. Figure 9 shows the various curvilinear coordinate systems arising from

different values of P. Here we supply without proof the following observations regarding the effect of varying P on V and its solution trajectories:

1. In the limit as $P \to \infty$, $V(p)$ approaches $N(\widetilde{p})$, where $\widetilde{p}$ is the point on C closest to p.
2. Where solution trajectories cross C in the normal direction, they remain parallel to that direction over longer distances for larger values of P.
3. Inversely, as P decreases, solution trajectories that cross C in the normal direction in general deviate more rapidly from the normal direction.

Using the Curvilinear Coordinate System While any point $(x, y) \in \mathbb{R}$ should have a corresponding coordinate $(s, t)_C$ in the curvilinear coordinate system induced by C, closed-form expressions for converting between the two coordinate systems would be difficult or impossible to find.

In practice what we wish to do is find the $(s, t)_C$ coordinates of many points (x, y). In our work, we solved the system (5) with initial condition $\vec{x}(0) = \vec{C}(s)$ for many values of s to produce many solutions starting from evenly spaced points along C. We solved the system both forwards and backwards in time to sufficiently cover the domain of interest and then concatenated the solutions. We then interpolated these solutions over the domain of interest, to assign to every point (x, y) the value of s such that $(x, y) = (s, t)_C$.

4.4 Results

We applied the texture-mapping procedure to both canine and rabbit ventricular endocardial surfaces with digitized canine Purkinje networks as the texture images. Details regarding these materials can be found in Section 3.

4.4.1 Canine Ventricles with Canine Purkinje Network

Left Ventricle The approximating curve chosen for the canine left ventricle is shown in Figure 10. From the plots, it can be seen at various cross sections perpendicular to the cylinder axis that the surface is well-approximated. Particularly near the septum wall, the cylinder closely approximates the true endocardial surface.

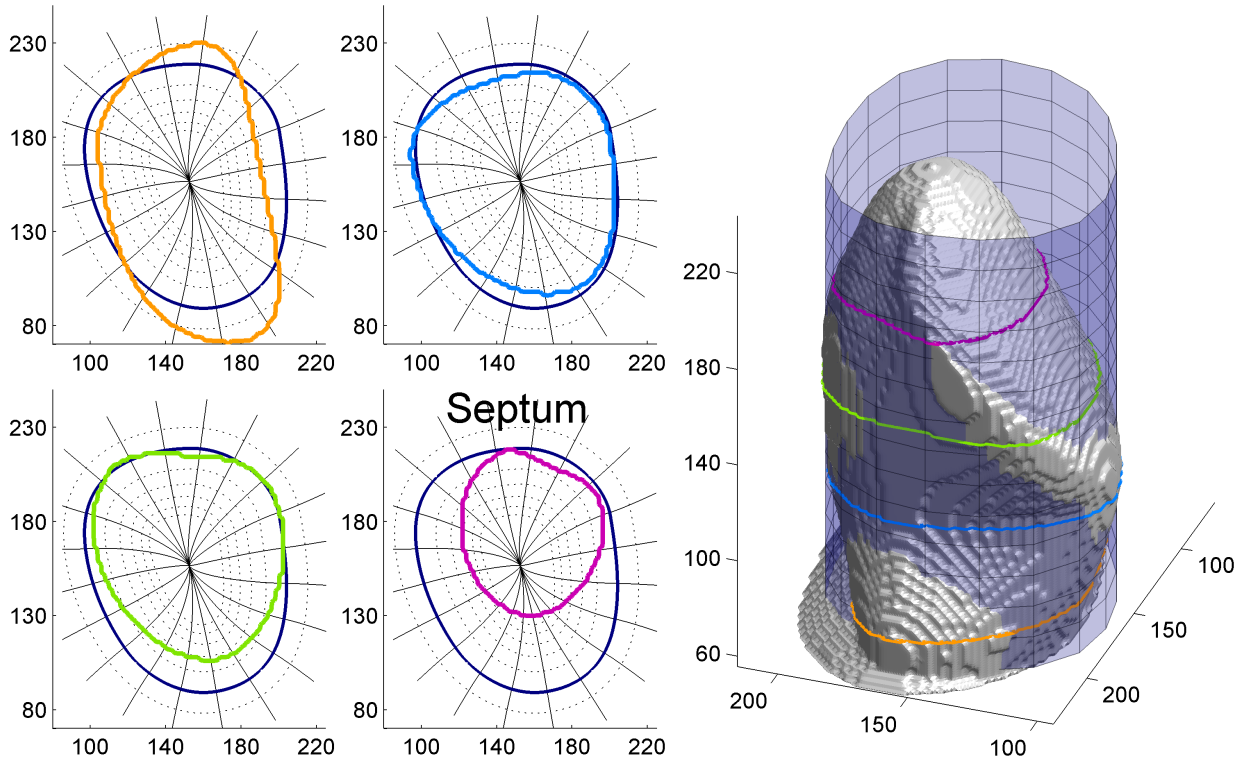

Figure 10: Visualizations of the canine left ventricular endocardial surface and the curve and associated cylinder chosen to approximate the surface. (**Left**) Plots show the chosen curve C and the resulting curvilinear coordinate system plotted against various contour lines from cross-sections of the endocardial surface. The chosen curve fairly well approximates the surface and its contour lines with agreement being best in the middle contours, or between the base and apex of the ventricle. The curve and contours coincide particularly well near the septum wall. (**Right**) Plot shows an isosurface of the endocardial surface (grey), the approximating cylinder (transparent) and the same contour lines used in the left plots superimposed onto the surface for reference. The view is facing the septum wall.

Figure 11 shows the results of texture mapping the left ventricular endocardial surface with the canine left Purkinje network (see Figure 2). The texture image was positioned such that the His Bundle connection was located near the middle of the septum wall, and the extent of coverage of the endocardial surface agrees well with the experimental photographs.

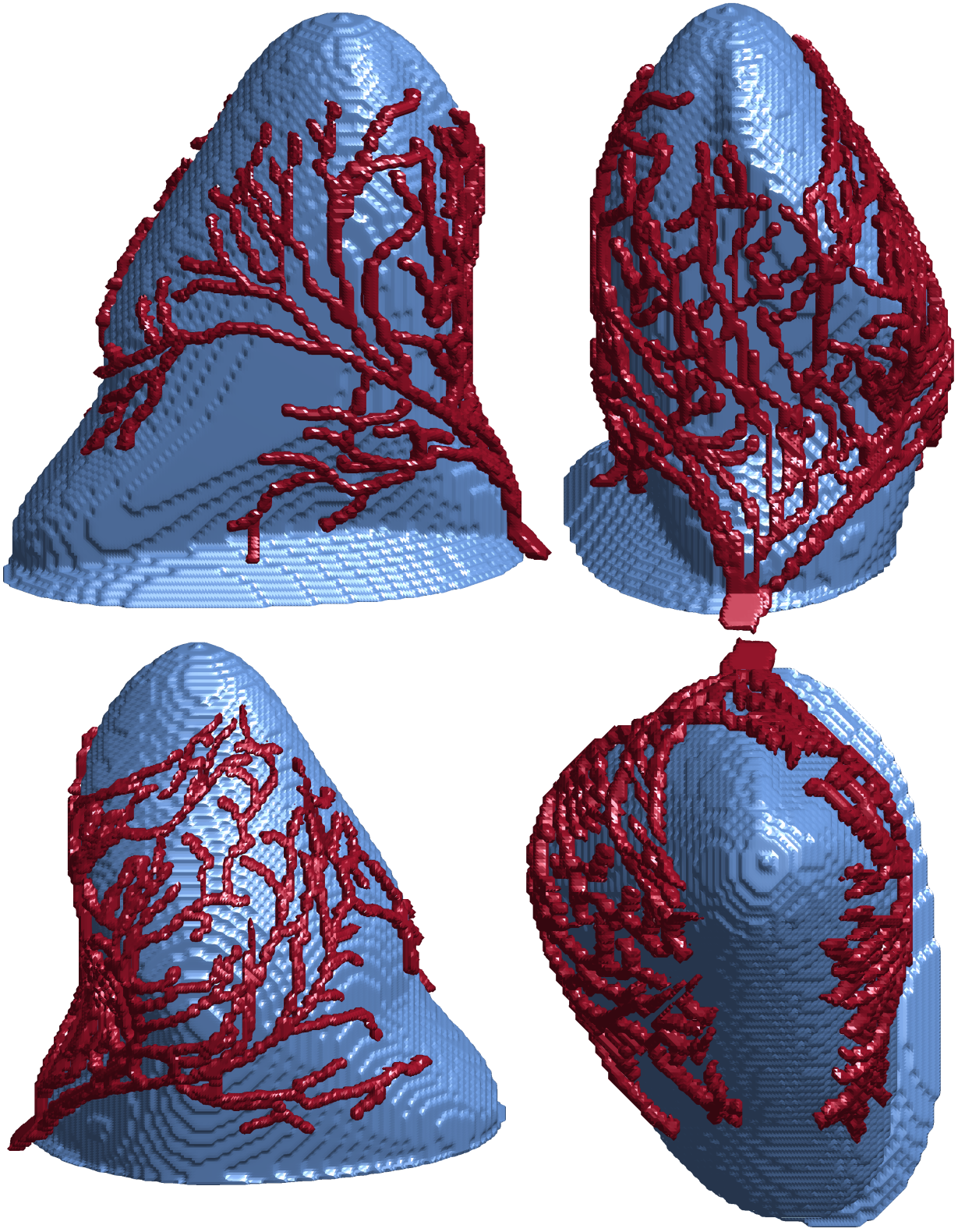

Figure 11: Visualizations of the texture mapping of the canine left Purkinje network onto the canine left ventricular endocardial surface. The extent of the texture-mapped network is nearly that of the entire endocardial surface.

The right ventricular endocardial surface has a distinctly different profile than that of the left ventricle. Figure 12 shows the approximating curve chosen for texture mapping. From the plots, it can be seen at various cross-sections perpendicular to the cylinder axis that the surface is well-approximated in the portion of the ventricles near the base. Particularly near the septum wall, the cylinder closely approximates the true endocardial surface. Near the apex, the cylindrical approximation does not closely follow the surface.

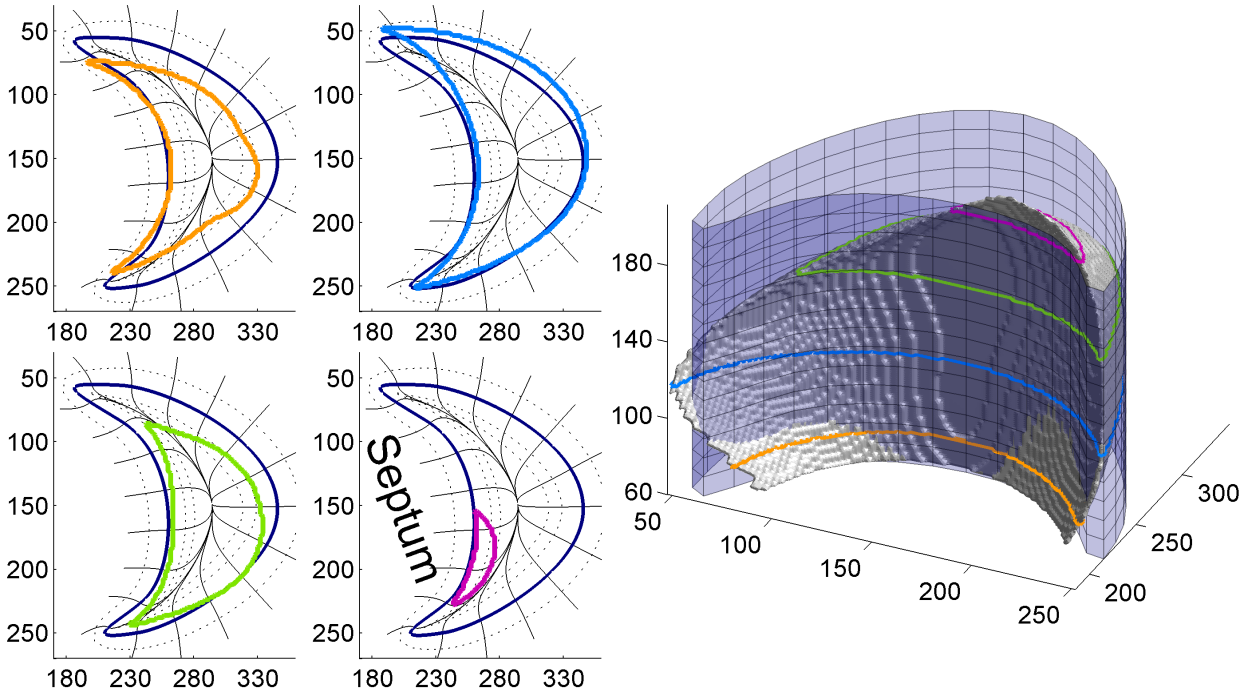

Figure 12: Visualizations of the canine right ventricular endocardial surface and the curve and associated cylinder chosen to approximate the surface. (**Left**) Plots show the chosen curve C and the resulting curvilinear coordinate system plotted against various contour lines from cross-sections of the endocardial surface. Contour lines from the endocardial surface have a distinctive crescent shape, where the inner curve corresponds to the septum wall. The chosen curve coincides closely with the septum wall in particular, and agreement is close elsewhere as well, but worsens near the apex. (**Right**) Plot shows an isosurface of the endocardial surface (grey), the approximating cylinder (transparent) and the same contour lines used in the left plots superimposed onto the surface for reference. The view is facing the septum wall.

Figure 13 shows the results of texture mapping the right ventricular endocardial surface. The digitized Purkinje network was positioned so as to coincide with the placement of the network as

shown in Figure 3. Specifically, the His Bundle connection was aligned with the the apparent 'seam' between the septum and free walls of the ventricle, and the network image was resized so as to encircle much of the endocardial free-wall surface and to cover most of the septum wall..

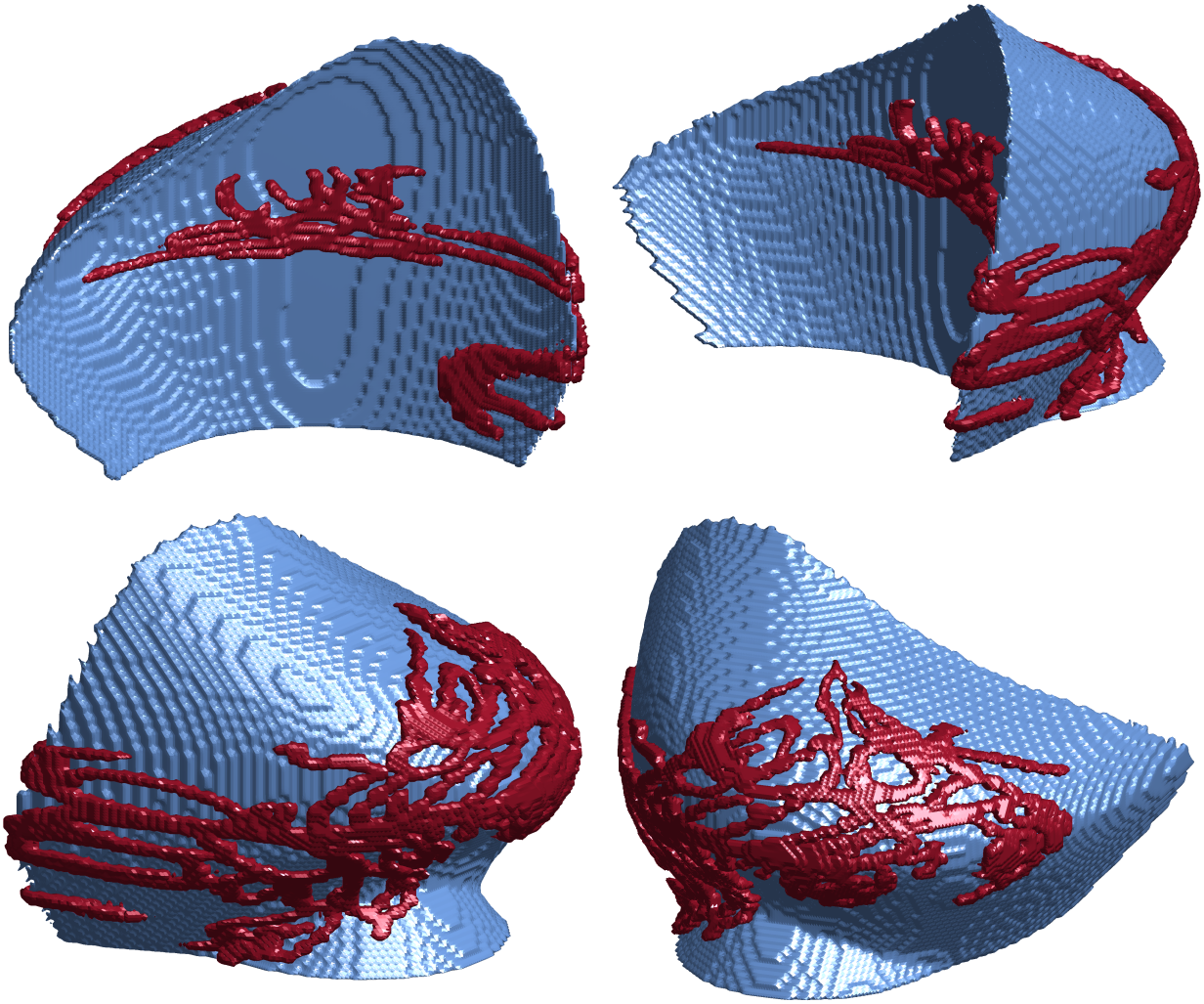

Figure 13: Visualizations of the texture mapping of the canine right Purkinje network onto the canine right ventricular endocardial surface. The extent of the network is limited. This coincides with experimental observations near the septum wall, but network coverage of the free wall is observed to be greater than achieved here, particularly near the apex.

4.4.2 Rabbit Ventricles

Our reference photographs of Purkinje networks (Figures 2 and 3) are of canine ventricles and we did not have access to rabbit Purkinje network photographs. We chose to emulate the place-

ment and coverage of the Purkinje networks in the canine ventricles when texturing the rabbit ventricles.

The approximating curve chosen for the rabbit left ventricular endocardial surface is shown in Figure 14. From the plots, it can be seen at various cross-sections perpendicular to the cylinder axis that the surface is well-approximated. Particularly near the septum wall, the cylinder closely approximates the true endocardial surface.

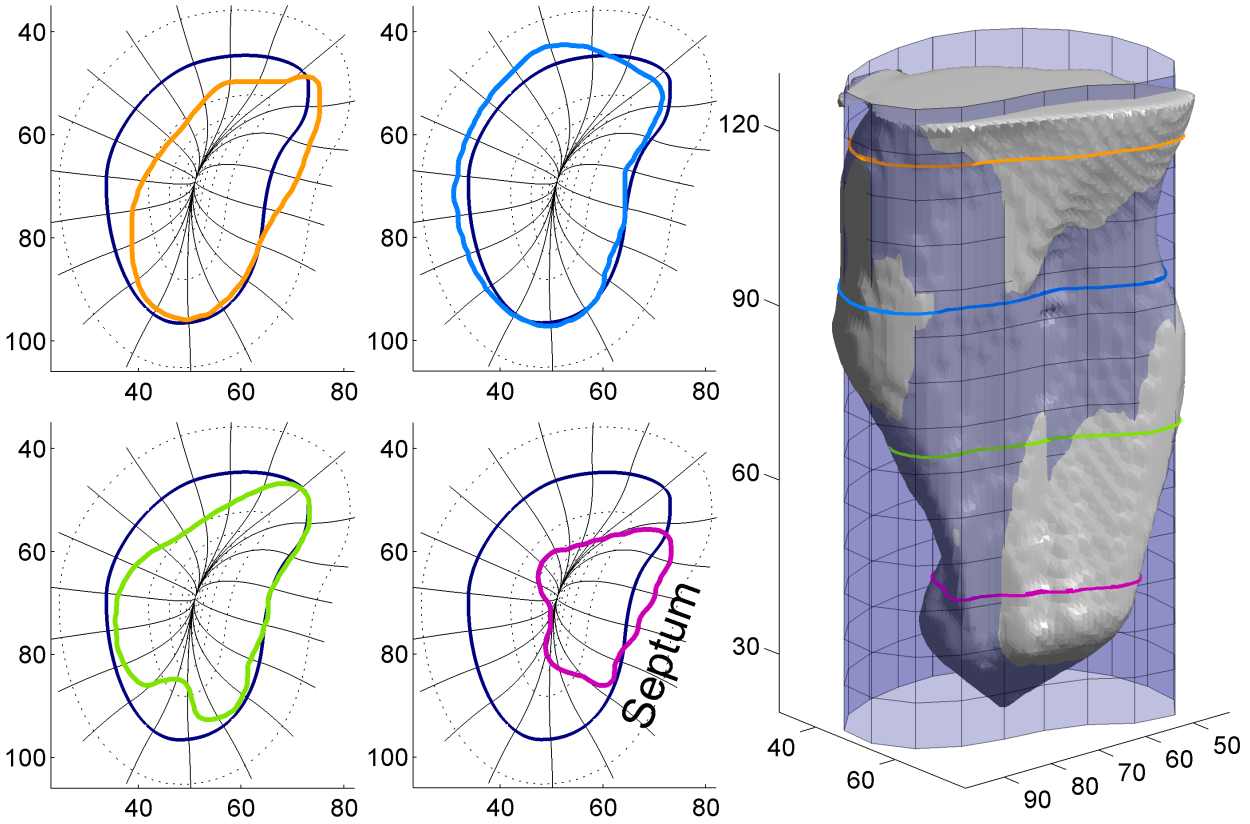

Figure 14: Visualizations of the rabbit left ventricular endocardial surface and the curve and associated cylinder chosen to approximate the surface. (**Left**) Plots show the chosen curve C and the resulting curvilinear coordinate system plotted against various contour lines from cross-sections of the endocardial surface. The curve coincides with the surface particularly closely near the septum wall and at the base of the ventricle. The approximation worsens nearer the apex. (**Right**) Plot shows an isosurface of the endocardial surface (grey), the approximating cylinder (transparent) and the same contour lines used in the left plots superimposed onto the surface for reference. The view is facing the septum wall.

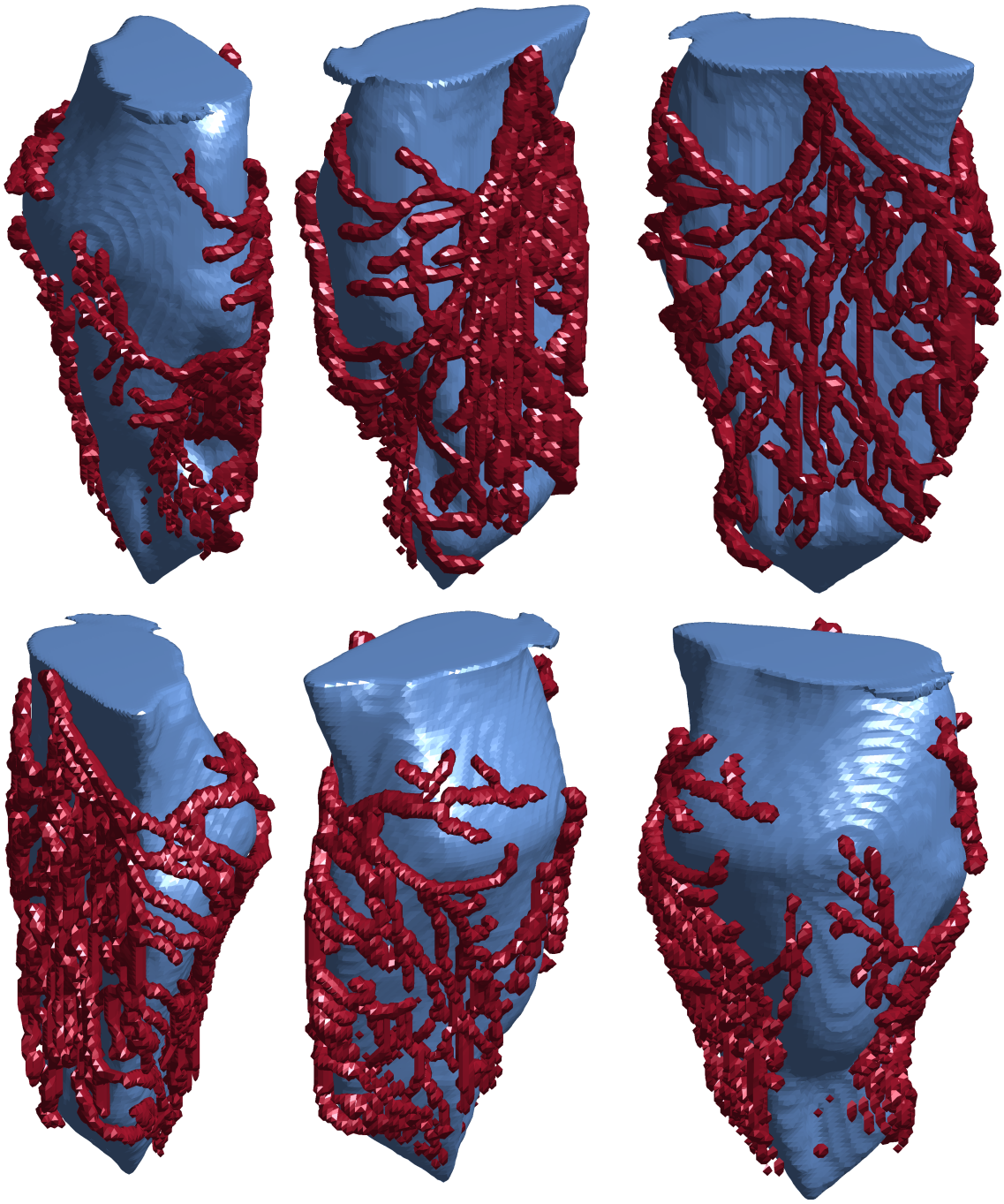

Figure 15: Visualizations of the texture mapping of the canine left Purkinje network onto the rabbit left ventricular endocardial surface. The extent of the texture mapped network is nearly that of the entire endocardial surface.

Figure 15 shows the results of texture mapping the left rabbit ventricular endocardial surface. The aspect ratio of the digitized network was altered significantly so that the extent of the texture

mapped network would cover nearly all of the endocardial surface, so as to coincide with experimental observations of Purkinje networks, as in Figure 2. The network was positioned so that the bundle branch originated near the center of the septum wall, and the network wrapped around the entire endocardial surface.

The approximating curve chosen for the rabbit right ventricle endocardial surface is shown in Figure 16. From the plots, it can be seen at various cross-sections perpendicular to the cylinder axis that the surface is well-approximated along much of the cylinder axis, particularly near the septum wall. Near the apex, the cylinder does not coincide with the surface as closely.

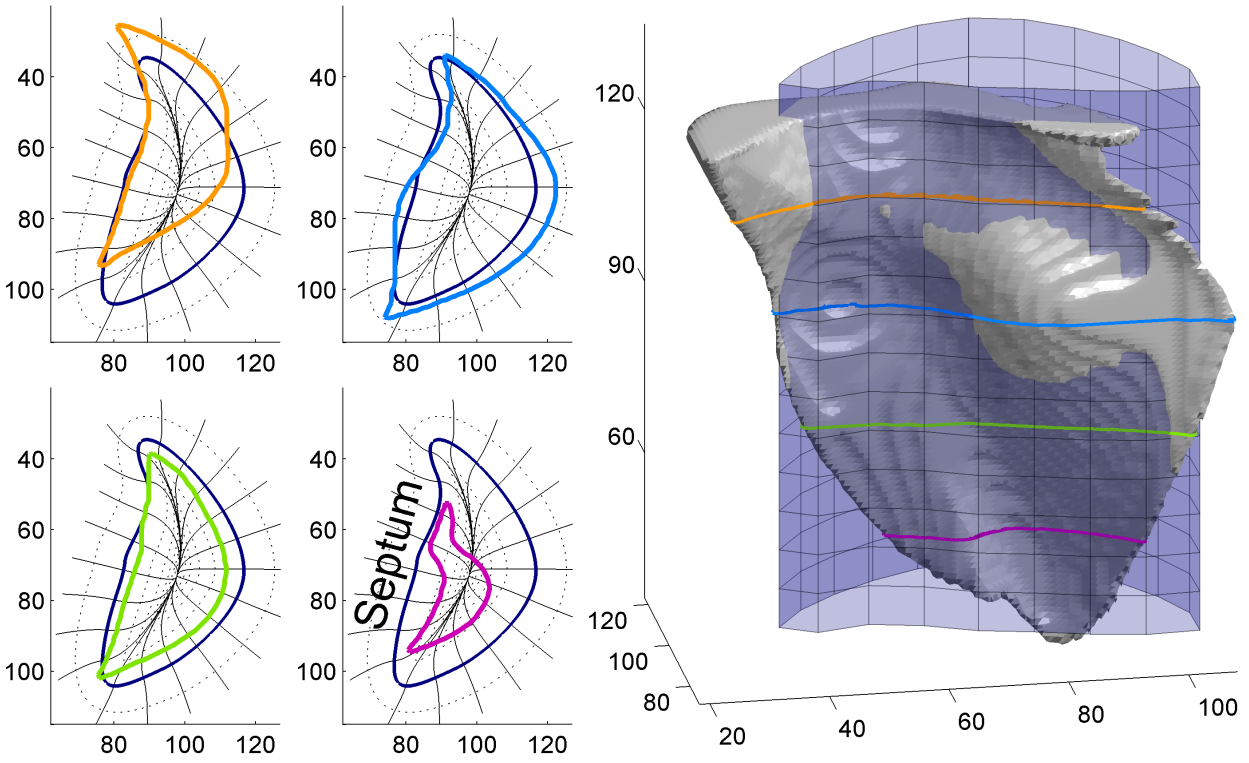

Figure 16: Visualizations of the rabbit right ventricular endocardial surface and the curve and associated cylinder chosen to approximate the surface. (**Left**) Plots show the chosen curve C and the resulting curvilinear coordinate system plotted against various contour lines from cross-sections of the endocardial surface. The curve coincides with the surface particularly closely near the septum wall and between the ventricle base and apex. The approximation worsens near both the apex and the base. (**Right**) Plot shows an isosurface of the endocardial surface (grey), the approximating cylinder (transparent) and the same contour lines used in the left plots superimposed onto the surface for reference. The view is facing the septum wall.

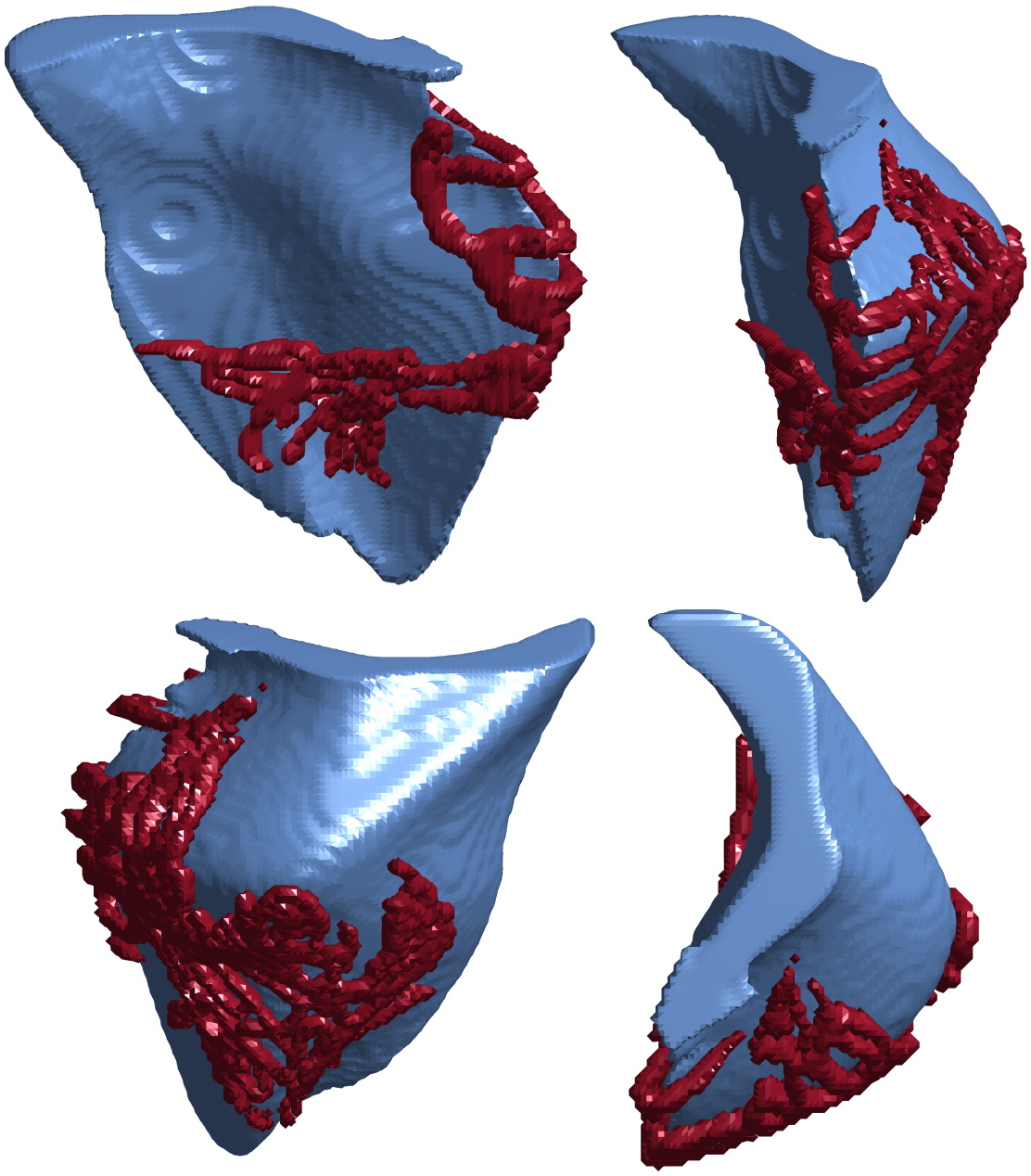

Figure 17: Visualizations of the texture mapping of a Purkinje network onto the rabbit right ventricular endocardial surface. The extent of coverage of the endocardial surface by the mapped network coincides with experimental observations.

Figure 17 shows the results of texture mapping the right ventricle endocardial surface. The Purkinje network was aligned so that the bundle branch coincided with one side of the septum wall, so as to coincide with experimental observation (see Figure 3).

5 Coupled Ventricle-Purkinje Systems

In this section we turn to the second major component of our work: modeling combined ventricular-Purkinje systems. The high-level strategy that we use in modeling these systems is to couple a ventricular model and a Purkinje model. We therefore begin this section with a review of the method we chose for implementing ventricles-only models: the phase-field method. The phase-field method is versatile and can also be used to represent other structures with non-trivial boundaries. In 2012 Cherry and Fenton developed a two-dimensional structural model of the Purkinje network and implemented it using the phase-field method [7], and we choose to use the same method here for modeling the three-dimensional Purkinje structure.

After reviewing the phase-field method and Cherry and Fenton's work, we present two new models we have developed for the ventricle-Purkinje system and discuss modeling concerns. Whereas the structural model that Cherry and Fenton developed utilized a very simplified ventricular structure, our models incorporate anatomically realistic ventricular data sets. The complicated three-dimensional structure of the ventricles makes the incorporation of a Purkinje network a much more difficult modeling task, and we use the texture-mapping approach presented in the previous section as a basis for this work.

We conclude this section with a presentation of results from our models. We discuss a test problem used to validate coupling between the ventricular and Purkinje systems, and then move to model implementations that incorporate anatomically realistic rabbit ventricular data sets. We validate our models by comparing activation times over the ventricles with experimental observations, and find that our models produce physiologically realistic results.

5.1 Prior and Foundational Work

Implementing ventricular models in which the cardiac reaction-diffusion equations are solved on anatomically realistic geometries requires methods for solving the equations and imposing no-flux boundary conditions on arbitrary, non-trivial domains. There are several popular approaches for implementing this type of model [8], such as finite differences, finite elements, and finite volumes. Depending on the representation of the anatomical data, some approaches are better or more natural choices than others. Here we use finite differences with the phase-field method for solving on arbitrary domains.

5.1.1 The Phase Field Method

The phase-field method is a method for solving problems involving an interface. Popular uses of the method involve problems where the interface boundary is changing, such as in dendrite solidification [4]. In 2005, Fenton et al. applied the phase-field method to solve cardiac reaction-diffusion equations on realistic heart geometries. In that work, and also here, the interface does not undergo any changes because the tissue and its boundary are regarded as static and unchanging.

The phase-field method models the interface by introducing an auxiliary scalar field over the domain, where points on either side of the interface (in the two different materials or phases) take on different values, and at the interface the value smoothly transitions in finite width. In the work done by Fenton et al., values of 1 and 0 were used, with 1 representing tissue and 0 representing empty space; here we use the same convention. The phase-field method then calls for a number of substitutions to be made to the PDE of interest in order to obtain a new PDE. For the system (3), the modified system complete with the phase field ϕ is given below by (6).

$$\phi \frac{\partial V}{\partial t} = -\phi \frac{I_{ion}}{C_m} + \nabla \cdot (\mathbf{D}\phi \nabla V) \tag{6}$$

5.1.2 Cherry and Fenton's 2D-2D Model

As was previously mentioned, in 2012 Cherry and Fenton created and implemented a coupled two-dimensional ventricular and Purkinje network model to study differences in arrhythmia dynamics where a Purkinje network is present [7]. A discussion of the results of their work can be found in Section 3; here we turn to issues regarding the implementation of their model.

The Cherry-Fenton ventricular-Purkinje model was created by coupling a Purkinje model based on experimental photos of Purkinje networks with a ventricular model consisting of a cylindrical patch of ventricular tissue. A schematic diagram of the model structure can be seen in Figure 18. The Purkinje model was implemented using the phase-field method, and the ventricular model was a two-dimensional patch of cardiac tissue with no-flux boundary conditions on two of the edges and periodic boundary conditions on the other two edges, resulting in a cylindrical geometry. Implementing similar boundary conditions in the Purkinje network was not necessary due to the tree-like structure of the digitized Purkinje network. A digitized Purkinje network extracted from experimental photographs served as the basis for the phase field used in the Purkinje model, and

the size of the ventricular tissue domain was chosen to match that of the domain in which the Purkinje network was embedded.

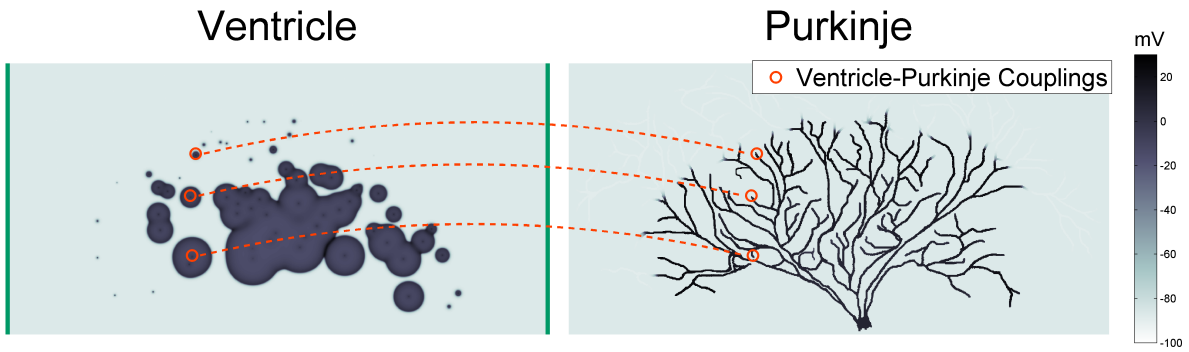

Figure 18: Results from Cherry and Fenton's coupled ventricle-Purkinje model, shown here to illustrate the coupling between the constituent ventricle and Purkinje models. Plots show ventricular tissue and Purkinje network 7 ms after the Purkinje network was activated; about half of the network coupling sites have been activated, and tissue is being activated by the network. Orange dashed lines show some of the many (130) ventricle-Purkinje coupling sites. Green lines at the sides of the ventricle plot indicate periodic boundary conditions; all other boundary conditions are no-flux.

The two models were both implemented using a finite-difference method with the same numerical grid. A forward-Euler method was used to solve the systems, and so membrane potential in the ventricular simulation, here called V_v, was updated at each time step according to the equation

$$V_v^{t+1}(i,j) = V_v^t(i,j) + dt\left[-\frac{I_{\text{ion}}}{C_m} + D\Delta V_v\right], \tag{7}$$

which is based on (3). Here ΔV_v is a discretization of the Laplacian of V_v at time t.

The two models were able to be coupled together in a relatively straightforward manner because both models were computed on the same numerical grid. Grid points corresponding to the end points of the Purkinje network fibers, where electrical coupling between the Purkinje and ventricle tissue occurs, were declared as 'two-way coupled,' and Equation (7) at those points was modified to become

$$V_v^{t+1}(i,j) = V_v^t(i,j) + dt\left[-\frac{I_{\text{ion}}}{C_m} + D\Delta V_v + D\Big[V_p^t(i,j) - V_v^t(i,j)\Big]\right] \tag{8}$$

where V_p is the membrane potential of the Purkinje system.

5.2 Model Development

We now present two models we have developed for the ventricle-Purkinje system. The first, which we have termed the 3D-3D model, represents both the ventricular and Purkinje systems in three dimensions. The 3D-3D model is a natural next step from the Cherry-Fenton 2D-2D model. Physically, both the ventricles as well as the Purkinje network are three-dimensional structures, and in terms of implementation coupling between the ventricular and Purkinje systems is easily handled by coupling of corresponding grid points.

The second model, which we refer to as the 3D-2D model, represents the ventricles in three dimensions and the Purkinje network in two dimensions. The development of the 3D-2D model is motivated by the fact that the Purkinje network is largely confined to the endocardial surface, and so is effectively a two-dimensional structure embedded in three dimensions. This permits the direct imaging of the Purkinje network through two-dimensional photographs, from which we can extract two-dimensional digitized Purkinje networks.

We hypothesised that a model that represented the Purkinje network as two-dimensional would reproduce all important dynamics observed in an analogous three-dimensional Purkinje network, and that the former model could provide several benefits. The first benefit that we considered was that of computational cost. Representing the sparse Purkinje network structure in two rather than three dimensions greatly reduces the number of node points in the numerical grid, and thus reduces the runtime of the model. Second, numerical solution of the Purkinje model on a numerical grid that is independent of the grid used for the ventricular model allows for the Purkinje network to be represented at a higher resolution than that of the ventricular model. The fine detail of the Purkinje structure can thus more accurately be represented without having to refine the resolution of the ventricular model.

5.2.1 3D-3D Model

The 3D-3D model is the natural extension of the Cherry-Fenton ventricle-Purkinje model. Figure 19 shows a schematic visualization of a 3D-3D model, illustrating the constituent models and where coupling between the models occurs. Whereas in their model Cherry and Fenton coupled together a two-dimensional ventricular and a two-dimensional Purkinje model, in the model presented here a three-dimensional ventricular and a three-dimensional Purkinje model are coupled together. The

key similarity between these two approaches is that both constituent models are computed on the same numerical grid. This leads to a straightforward means of achieving electrical coupling: defining a number of grid points as two-way coupled, allowing the two models to influence each other at a number of discrete sites.

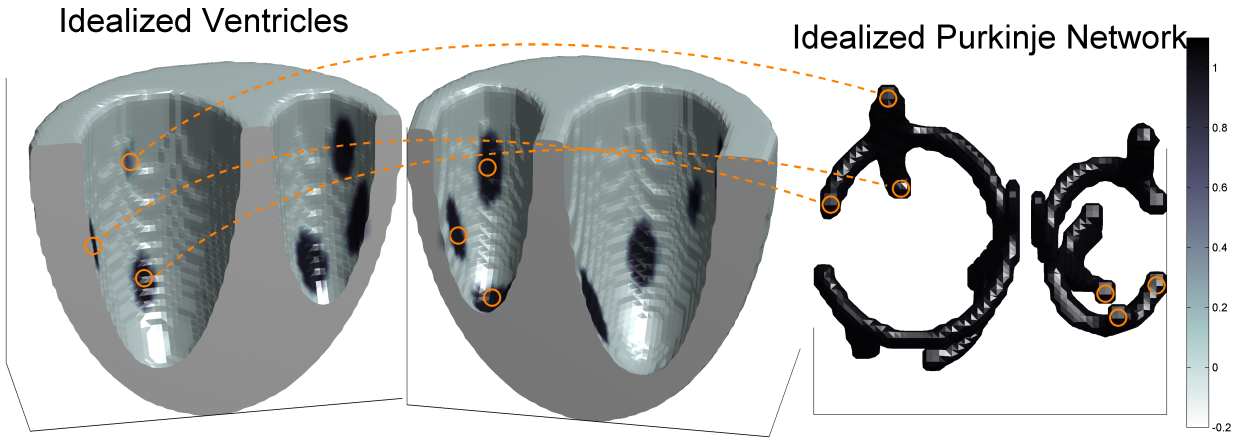

Figure 19: Schematic visualization of a 3D-3D model. The structure is a simplified contrived structure used for illustrative and test purposes only and is not anatomically realistic. (**Left**) View of the test geometry. (**Right**) View of the conduction system test geometries. Dashed lines show some of the many couplings between Purkinje networks and the ventricles.

Both the ventricular and Purkinje models use the phase-field method, and thus a scalar phase field representing the ventricular structure and another representing the Purkinje network are required. Several data sets exist upon which the ventricular phase field can be based, but the same cannot be said of the Purkinje network. Indeed, the reason for our work in the previous texture-mapping section is to make possible the reconstruction of a three-dimensional Purkinje structure. Using the texture-mapping method described in the previous section, we obtain a three-dimensional Purkinje network compatible with the ventricle model. Using our texture-mapping procedure, we are also able to map the locations of the endpoints of the fibers in the Purkinje network. The grid points onto which endpoints of the fibers are mapped then become the coupling sites between the two models.

5.2.2 3D-2D Model

The 3D-2D model for the coupled ventricle-Purkinje system combines a three-dimensional ventricular model with a two-dimensional Purkinje model. Because the three-dimensional Purkinje network was derived from texture-mapping a two-dimensional image onto a surface, another plausible strategy for simulating a coupled ventricular-Purkinje system is to simulate the ventricles in three dimensions but the Purkinje network in two dimensions - the native dimensions of the digitized Purkinje networks. Figure 20 shows a schematic visualization of a 3D-2D model, illustrating the constituent models and where coupling between the models occurs. This modeling approach differs in an important way from the Cherry-Fenton 2D-2D model and the previously discussed 3D-3D model in that the ventricular and Purkinje models necessarily do not occupy the same space.

The implementation for both constituent models remains largely the same as that of the 3D-3D model, but the means by which the two models are coupled together is significantly different. Whereas in the previous approach, both the ventricles and the Purkinje network were represented in the same space, here they are not. Thus, the straightforward means of defining some grid points (on which all models are being computed) as two-way-coupled cannot be applied to couple the models together. Here we essentially discard the texture-mapped Purkinje network except for the locations of the coupling sites. Coupling is implemented between the location of the coupling site in the 2D Purkinje network and the location on the ventricular surface of that point under the texture map.

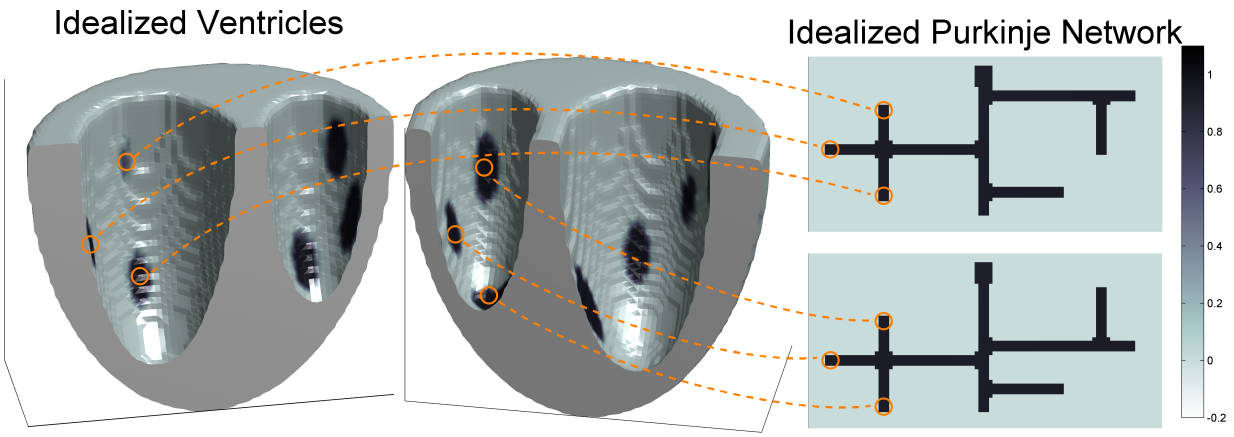

Figure 20: Schematic visualization of a 3D-2D model. The structure is a simplified contrived structure used for illustrative and test purposes only, and is not anatomically realistic. (**Left**) View of the test geometry. (**Right**) View of the conduction system test geometries. Dashed lines show some of the many couplings between Purkinje networks and the ventricles.

5.3 Implementation Considerations (3D-3D and 3D-2D)

Choice of Cardiac Model The choice of cardiac cell model depends on a number of factors, such as the research aim and available computing resources. The model can affect many dynamics relating to arrhythmia, such as conduction velocity, alternans, and spiral and scroll wave dynamics. As a first step in validating our model, we sought to synchronize activation times of the ventricle tissue with that of experimental findings. To realistically represent activation times, only a simple cardiac model is needed in order to capture the key aspects of the depolarization wavefront. For this reason we used the two-variable Mitchell-Shaeffer model [23].

The Phase-Field Method: Maintaining Connectivity The exact means by which the phase field was calculated in our work is the same as that used by Fenton et al. [14]: a relaxation method that took as an input a Boolean mask with the form of an indicator function, with 1 representing tissue and 0 representing empty space. The relaxation method was implemented by the partial differential equation (9).

$$\frac{d\phi}{dt} = \xi^2 \Delta\phi - G'(\phi) \tag{9}$$

Here ξ is the interface width and G is a dual-well potential function with minima at $\phi = 0$ and $\phi = 1$ – the values of the two domain phases – defined as

$$G(\phi) = -\frac{(2\phi - 1)^2}{4} + \frac{(2\phi - 1)^4}{8}.$$

The phase-field method can represent only domains with sufficiently coarse detail. That is, for phase-field implementations on a finite-difference grid, the resolution of the phase field must be coarser than that of the grid spacing. In the case of representing the Purkinje network, this can pose a significant problem, due to the fine detail of the network.

The Purkinje phase fields used in our work were calculated with input masks taken to be the digitized Purkinje networks discussed in section 3. The digitized Purkinje network was in some areas only a single pixel or grid point wide, and so the smoothing procedure in some cases compromised the connectivity of the network. Figure 21 shows an example of a contrived domain that exhibits these qualities: the thin annular domain loses connectivity under the relaxation procedure.

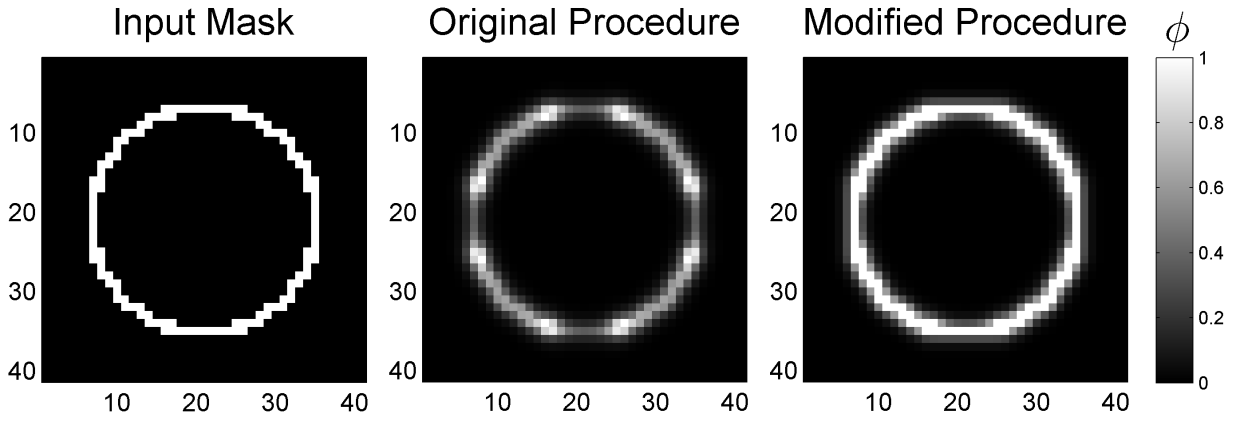

Figure 21: Comparison of phase fields resulting from the original and modified relaxation algorithm. The original mask has a grid spacing of $\Delta x = .1$, and both phase-field generation methods are run with the interface width $\xi = .2$. (**Left**) The Boolean input mask defining a thin annular domain. (**Center**) The phase field resulting from the application of the original relaxation algorithm to the input mask. Note that the top, bottom, left, and right parts of the annulus have low ϕ values, which compromises the connectivity of the domain. (**Right**) The phase field resulting from the application of the modified relaxation procedure with the added boundary condition. The entire original annular region has a value of $\phi = 1$, ensuring connectivity.

To ensure that connectivity was preserved in the phase field, we modified the smoothing procedure

by imposing an additional boundary condition. The modified condition was that $\phi = 1$ on the boundary of Ω, the domain of points with $\phi = 1$ in the original mask. In terms of implementation this is easily achieved: if the relaxation procedure is implemented with forward Euler or a similar method, then $d\phi/dt = 0$ for any point where $\phi = 1$.

Implementing Coupling A number of different approaches can be used to implement coupling between the ventricle and Purkinje models. The most straight-forward case is where both the ventricular and Purkinje models are of the same dimensionality and are computed on the same numerical grid. In models such as the Cherry-Fenton ventricle-Purkinje or the 3D-3D model presented here, specific nodes on the numerical grid are declared as two-way coupled between two models.

Implementing this in a program can be done easily by introducing an auxiliary Boolean coupling matrix of the same dimensionality and size as that of the numerical grid. The coupling matrix is a sparse structure, where a non-zero entry indicates that the grid point is two-way coupled between the two models of interest. In cases where there are actually three models (one for the ventricles and one for the left and right Purkinje network branches) two coupling matrices will be required, given that coupling only occurs between the ventricles and the Purkinje network.

In the case of coupled models of differing dimensionality, this approach cannot be applied in a straightforward manner and must be adapted. Here, a numerical grid point (x, y, z) in three-dimensional space must be coupled to a grid point (i, j) in two-dimensional space. To extend the coupling-matrix approach, we implemented two coupling matrices, one for each of the two models. The coupling matrix for the three-dimensional model is four-dimensional, where the first three dimensions correspond to the size of the numerical grid over which the three-dimensional model is computed, and the fourth dimension stores two values – the (i, j) coordinate in the two-dimensional model to which this (x, y, z) point is coupled, if it is coupled at all; if it is not coupled, then the entries are simply 0. The coupling matrix for the two-dimensional model is defined in much the same way: having three dimensions, the first two of which correspond to its numerical grid and the third holding the three coordinates of the correspondingly coupled grid point in the three-dimensional model, if applicable.

An alternate approach is to store the coupling sites in a list, and at each iteration in the time loop, to make the appropriate updates to the ventricle and Purkinje network state variables at the

indices in the list. Such an approach most likely will demand less storage space in memory than the coupling matrix approach but may be less readily parallelized.

Propagation at Coupling Sites Propagation of the depolarization wavefront between the ventricle and Purkinje models sometimes was blocked. Cherry and Fenton found in their work that defining only one grid point at each coupling site was insufficient to ensure propagation and so instead coupled four grid points arranged in a 2×2 array at each of the coupling sites. In our work, we found that one grid point was sufficient in many cases. It is likely that factors such as the diffusivity parameter, numerical parameters, or the cardiac cell model used have an affect here; for instance, a relatively large diffusivity results in the lower membrane potential around the coupling site, overwhelming the effect of coupling.

An issue that arose in our work was that the ventricular phase-field value also had a significant affect on whether coupling with one grid point would be sufficient to ensure propagation. We found that propagation occurred most reliably when the value of the phase field was close to 1. For this reason we ensured that in reconstructing the Purkinje networks used in simulation, the thin-shell endocardial layers we selected for texturing lay within that volume of the phase field exceeding a given value (such as $\phi > .9$).

Isolating the Thin-Shell Endocardial Layer In data sets containing the full ventricular structure, it is necessary to isolate a thin shell (the endocardial layer) in order to proceed with texture mapping. In our work, the ventricular data sets with which we began work were already in the form of phase fields. To isolate a thin shell, we began by isolating the ventricular chamber, based on taking that volume of the phase field below a given threshold (such as $\phi = .5$) within the chamber. This resulted in a Boolean tensor of grid points that lay within the chamber. We then applied a three-dimensional convolution with a spherical kernel and took all entries with value greater than 1, resulting in a tensor of the same size. This resulting tensor represents a volume expanded from that within the ventricle chamber, overlapping the ventricle tissue by a width of approximately the radius of the spherical kernel. A thin shell is obtained by taking those nonzero entries in this tensor that also satisfy some threshold value in the phase field.

Numerical Parameters In the 3D-3D model, all constituent models were computed on the same numerical grid, with the same uniform grid spacing being used in each model. In the 3D-2D model, models were computed on potentially different and sometimes non-uniform grids, and so consideration must be given to ensure that grid spacings are chosen to accurately represent the physical situation.

In cases where the aspect ratio of the digitized Purkinje network was not preserved, we implemented the 2D model with non-uniform grid spacing. Where a subset of the approximating cylinder given in the curvilinear coordinate system by $[a, b] \times [c, d]$ was selected as the portion of the cylinder on which the texture image was to reside, we defined the grid spacings $\Delta_P x$ and $\Delta_P y$ of the Purkinje network by

$$\Delta_P x = \frac{\Delta_V x(b-a)}{W} \qquad\qquad \Delta_P y = \frac{\Delta_V x(d-c)}{H}$$

where $\Delta_V x$ is the grid spacing used in the ventricles model (which we always took to be uniform), and W and H being the width and height of the digitized Purkinje network image, respectively.

5.4 Results

5.4.1 Test Problem

We developed a test problem in order to validate our program implementations. Here, both the ventricular and Purkinje network structures are contrived, highly-stylized constructs used only for the investigation of the models. We present these results for illustrative purposes, to compare the two method (3D-3D and 3D-2D) implementations, and to familiarize the reader with means of interpreting results.

Ventricles Structure The contrived ventricular structure of the test problem consisted of a half-ellipsoidal volume with two smaller half-ellipsoidal volumes removed to emulate the left and right ventricle chambers. Figure 22 shows isosurface plots of the test problem structure along with the isolated endocardial layers onto which the Purkinje network mapping was done.

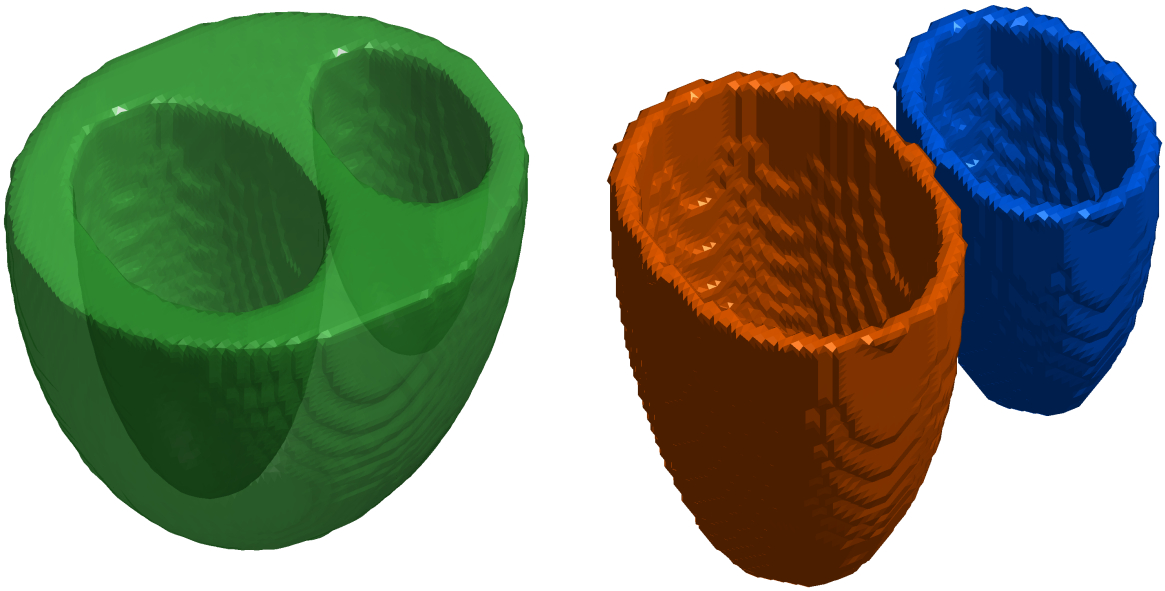

Figure 22: Test structure used in the test problem. (**Left**) The entire test structure – a half-ellipsoidal volume with two smaller ellipsoidal volumes removed to represent the ventricular chambers. (**Right**) The isolated layers used in the texture mapping.

Purkinje Networks The conduction system used in the test problem was an extremely simplified branching structure and served mainly to test the coupling between main structure and conduction system models. Due to the low number (7) of coupling sites, coupling was easily verified visually at each of the coupling sites from visualizing simulation results.

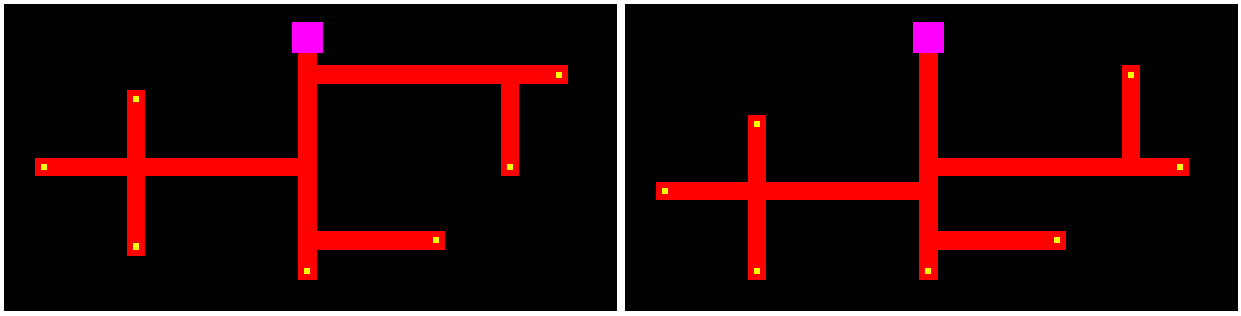

Figure 23: Diagrams showing the conduction systems used in the test problem. These simple contrived networks serve to validate model coupling and are not meant to model the genuine Purkinje network structure. Red represents the network, yellow the coupling sites, and magenta the stimulus sites. (**Left**) Left Purkinje network. (**Right**) Right Purkinje network.

Numerical Parameters For the test problem, we used a uniform grid spacing of $\Delta x = 0.05$cm in the main structural model and in the conduction system models of the 3D-3D model. The left conduction system network branch was applied to a 105×45 area of the left approximating cylinder, and so correspondingly values of $\Delta x = 0.525$cm and $\Delta y = 0.045$cm were used for the grid spacing of that model component. The right conduction system network branch was applied to a 74×45 area of the right approximating cylinder, and so values of $\Delta x = 0.037$cm and $\Delta y = 0.045$cm were used in the grid spacing of that model.

Other important numerical parameters include that the main time step used in the model was $dt = 0.02$ms. Because of the considerably faster action of the conduction system, those models were solved with a time step of $dt = 0.02/8 = 0.0025$ms by iterating them 8 times for every iteration of the ventricles model. This implementation is consistent with an operator-splitting approach.

Though our realistic anatomical models had associated fiber orientation data, we did not create such sophisticated data for the test problem. Instead, we assumed a vertical fiber direction in the ventricles with a conduction velocity of 0.001cm/s in the parallel and 0.0002cm/s in the direction perpendicular to the fibers.

Stimuli were applied for 4ms and full activation of the ventricles was achieved in around 90ms.

Results Our main goal in the implementation of the test problem was the verification of model coupling in the 3D-3D and 3D-2D model implementations. By using a simplified conduction system with a small number of distinct coupling sites, coupling could be verified simply by visualizing simulation output. Figure 24 shows results from the 3D-3D test problem model. Plots show isochronal maps of the activation times of the main structure; colors indicate at what point (time) in the simulation each point on the tissue was activated. Seven distinct primary sources of activation can be seen in each ventricle in the isochronal maps, indicating each of the seven coupling sites successfully activated a region of each ventricle. Figure 25 shows isochronal plots of results from the test problem 3D-2D model implementation. Here we again see seven distinct primary activation sites in each ventricle.

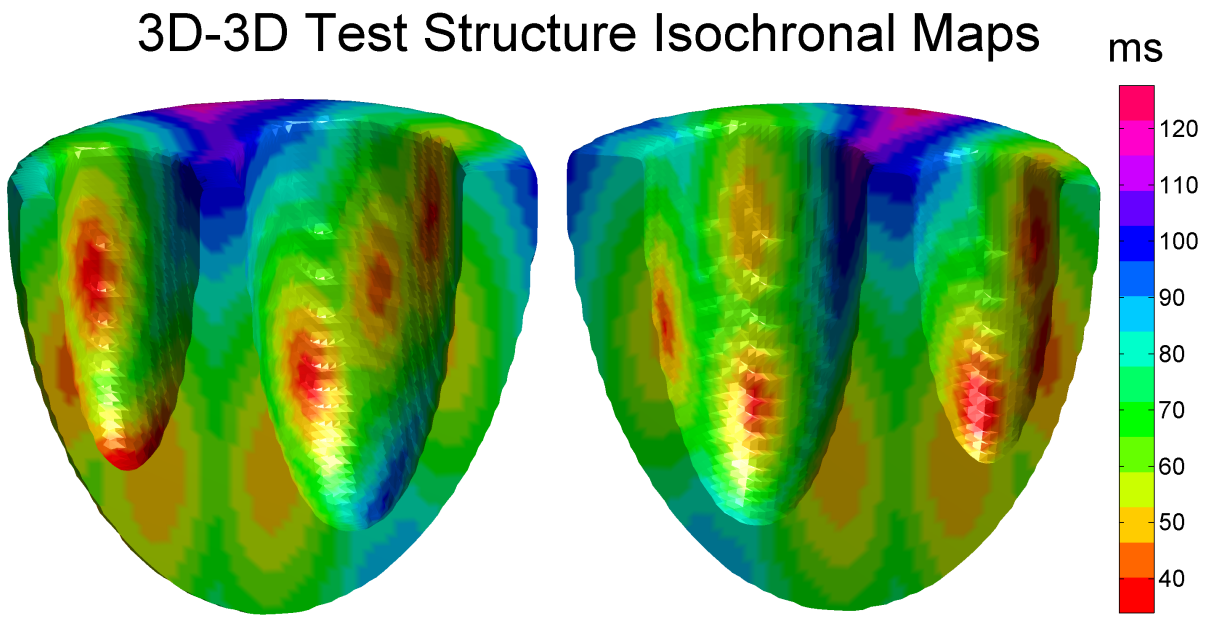

Figure 24: Activation times of the main structure in the test 3D-3D model. Plots show isochronal maps of activation times in a split view.

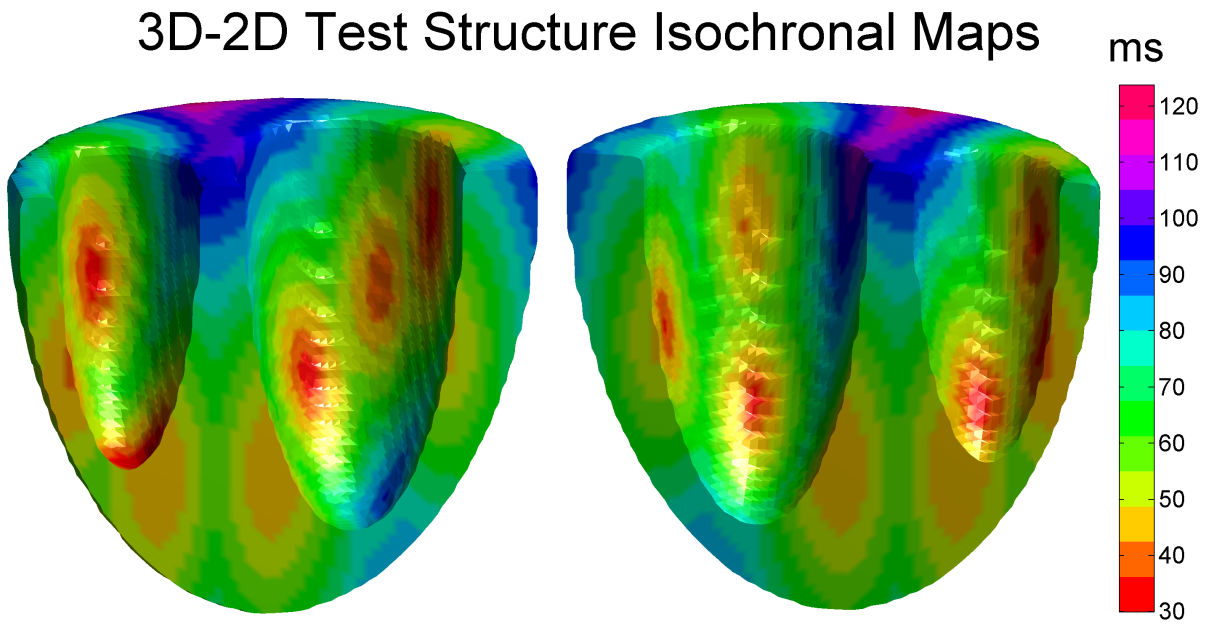

Figure 25: Activation times of the main structure in the test 3D-2D model. Plots show isochronal maps of activation times in a split view.

Model Comparison Early results with the test problem show that the 3D-3D and 3D-2D models can produce very similar activation sequences. Figure 26 shows plots of differences in activation times between the 3D-3D and 3D-2D test model implementations. Activation times are within 6 ms at all points in the tissue.

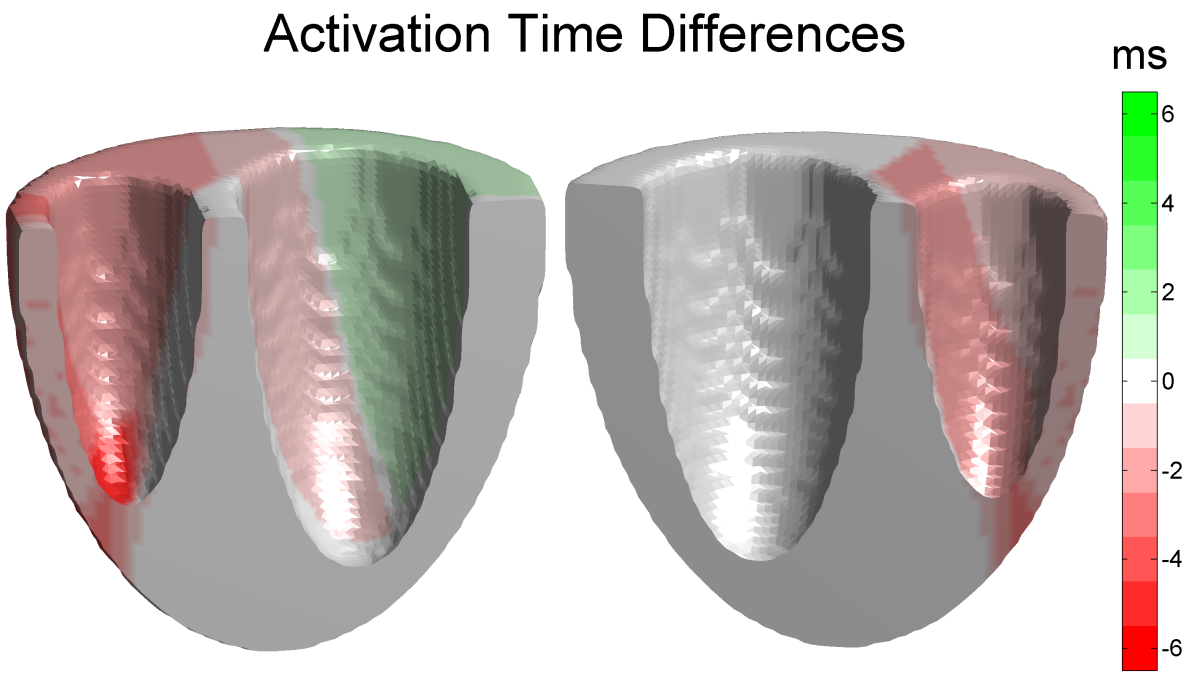

Figure 26: Comparison of activation times in the 3D-3D and 3D-2D model implementations of the test problem. Plots show at each point in the tissue the activation time of the 3D-3D model minus the activation time of the 3D-2D model. Colors are given so that white areas indicate near agreement of the two models, green indicates a positive difference (3D-2D has earlier activation), and red a negative difference (3D-3D has earlier activation).

5.4.2 Rabbit Ventricles with Canine Purkinje

We next implemented the 3D-3D and 3D-2D models with a realistic rabbit ventricular structure and with digitized canine Purkinje networks. Details of the structure and network digitizations can be found in Section 3.

3D-3D Results Results from the 3D-3D model can be seen in Figure 27. Plots show isochronal maps of the activation times of the ventricles; colors indicate at what point in the simulation each

point on the ventricles were activated.

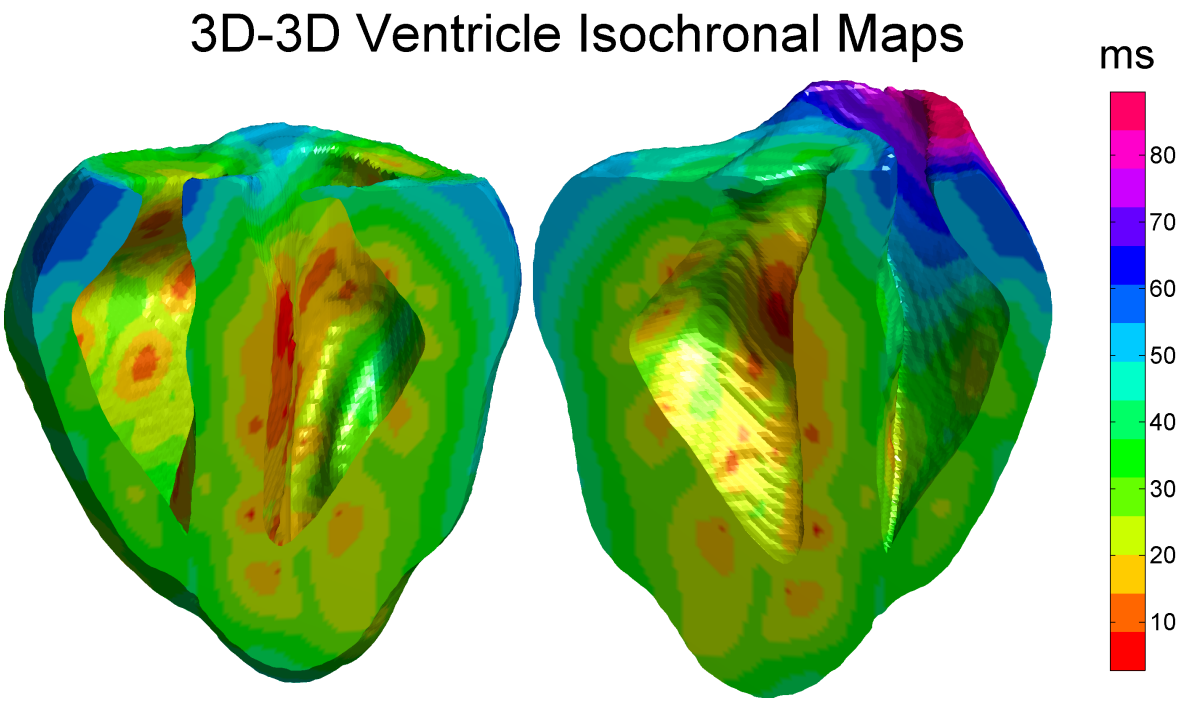

Figure 27: Isochronal plots showing activation times of the rabbit ventricles in the 3D-3D model.

3D-2D Results Figure 28 shows results from the 3D-2D model. Plots show isochronal maps of the activation times of the ventricles; colors indicate at what point in the simulation each point on the ventricles were activated.

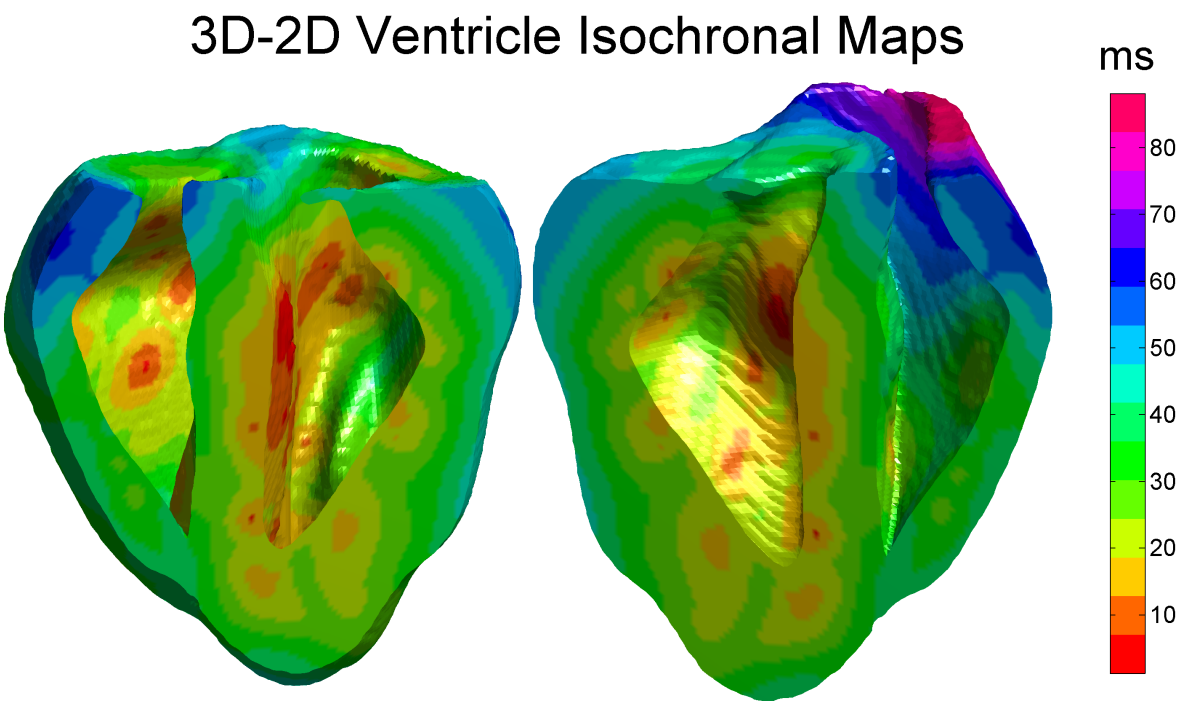

Figure 28: Isochronal plots showing activation times of the rabbit ventricles in the 3D-2D model.

Comparison with Experimental Observations The 3D-3D and 3D-2D models that were implemented using the Purkinje structures obtained through texture mapping matched well with experimental observations. The primary activation sites found by Durrer et al. are the septum and anterior walls of the left ventricle endocardium, with the right ventricle free wall being activated last [11]. Comparing isochronal maps of real (Figure 1) and simulated (Figures 27 and 28) activation times from our models, we find that our results reproduce many of the important characteristics of a genuine heart activation sequence.

Model Agreement Figure 29 shows differences in activation times of the ventricles between the 3D-3D and 3D-2D models. The two models show very similar activation times that deviate by only several milliseconds.

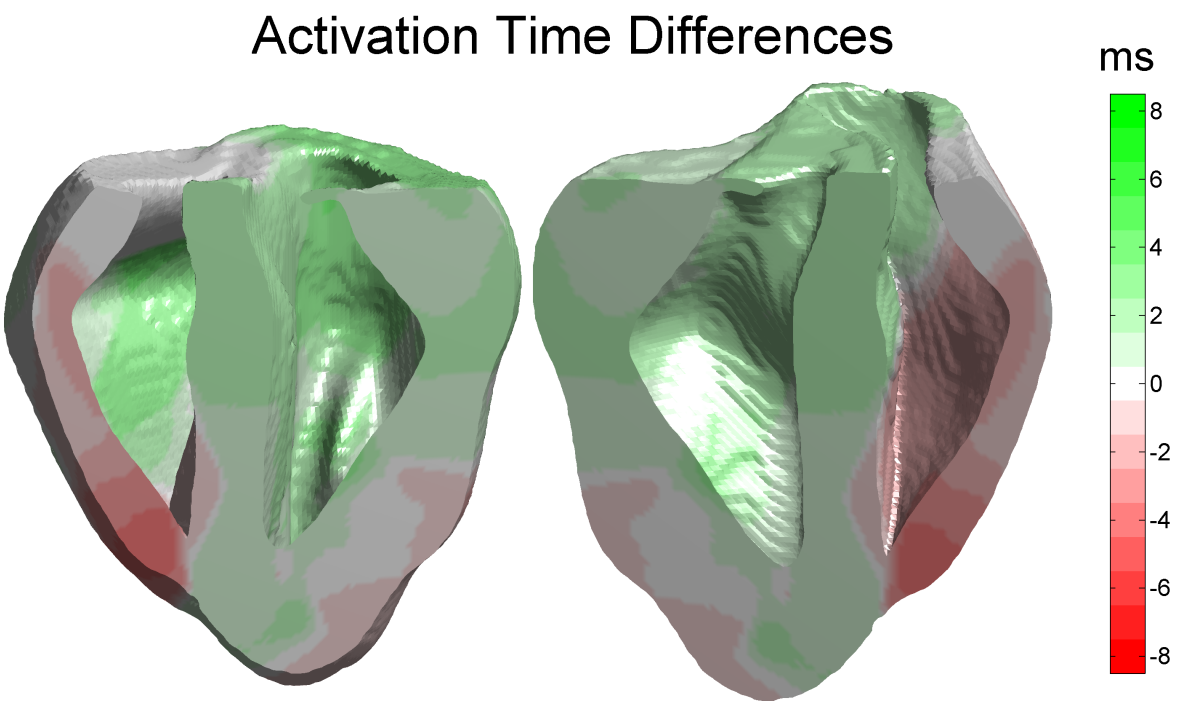

Figure 29: Comparison of activation times in the rabbit ventricles in the 3D-3D and 3D-2D model implementations. Plots show difference in activation times of the ventricles between the 3D-3D and 3D-2D models.

6 Discussion

Anatomically Realistic Purkinje Networks In applying our texture-mapping technique to produce three-dimensional Purkinje networks, our goal was to produce anatomically realistic structures. The position and extent of coverage on the endocardial surfaces are important features of the network, particularly to our goal of achieving realistic activation times of the ventricles by excitation of the Purkinje structure. To validate the network structures we obtained, we compare them to the experimental photographs from which the Purkinje network structures were extracted.

Figure 2 shows the original experimental photographs of the left canine ventricle as well as a modified photograph in which the digitized left Purkinje network branch structure is overlaid the original photograph. The positioning and extent of the left branch of the Purkinje network is most easily described in reference to the His Bundle connection, or left bundle branch, which is located in the photograph near the top of the image. Physiologically, the bundle branch is the source of all Purkinje fibers and is located on the septum wall. The means by which the left ventricle was dissected involved a cut opposite to the septum wall, which is why the bundle branch is in the center of the resulting photograph. The Purkinje network spreads outward from the bundle branch, and fibers evenly cover most of the endocardial surface. The network is quite symmetric in its coverage, with fibers reaching the free wall (along which the dissection was made) from both directions.

In texture mapping the left ventricle endocardial surfaces, we aimed to reproduce these physiological features. Figures 11 and 15 show mappings of the left Purkinje network onto canine and rabbit left ventricle endocardial surfaces. The networks were positioned to cover the entire endocardium, and the bundle branch was positioned on the septum wall.

Figure 3 shows the original experimental photographs of the right canine ventricle as well as a photograph in which the digitized right network structure has been overlaid. Here the dissection method is significantly different from the one used in the left ventricles; the right ventricle was cut along the 'seam' between the septum and free wall. The photograph shows the endocardial surface corresponding to the septum on the left, and the free wall endocardial surface on the right. The overall network structure of the right Purkinje branch is much less symmetric than the left Purkinje branch both visually and from a physiological perspective. The right Purkinje network branch still begins at the bundle branch, but in this case the bundle branch is not positioned at the middle of

the septum wall. Instead, it is positioned at the other septum and free wall seam. The network coverage of the septum endocardial surface is limited, with fibers only appearing near the apex. The free wall is covered extensively in network fibers much like the left ventricle.

In texture mapping the right ventricular endocardial surfaces, we aimed to reproduce these physiological features. Figures 13 and 17 show mappings of the right Purkinje network onto canine and rabbit right ventricular endocardial surfaces. The positioning of the bundle branch along the seam of the septum and free wall was a key concern, followed by the extent of coverage by the network.

We conclude that the texture-mapped Purkinje networks that we constructed in Section 4 achieve realistic coverage of the endocardial surfaces. The texture-mapped networks thus represent well the three-dimensional Purkinje network structure with respect to anatomical realism.

Ventricular Activation Times The three-dimensional Purkinje structures recovered through texture mapping were used as a conduction system in the development of models of the ventricular system. Our goal was to create a model that reproduced key features of the real cardiac conduction system. In particular, the overall progression of the total depolarization (activation) of the ventricles, termed the activation sequence, has been well-characterized [11]. A physiologically realistic model must reproduce this activation sequence.

Figure 1 shows results from the characterization done by Durrer et al. of the activation sequence of the human heart. The figure shows isochronal plots of the activation of the ventricles. Key features of the activation sequence are those areas that are first to depolarize. Activation begins in the left ventricular endocardial surface, particularly near the septum wall. The last region to depolarize is the right ventricular free wall.

Figures 27 and 28 show plots similar in layout to Figure 1: isochronal plots of the activation times achieved in our model. Key features of our results are that the left ventricular endocardium contains some of the sites of earliest activation, particularly near the septum. The right ventricular free wall is also the last region to depolarize, matching with experimental observations. In addition to achieving a realistic activation sequence, the entire activation of the ventricles occurs in realistic time [11].

6.1 Limitations

Cylindrical Approximation The texture-mapping procedure presented here relies heavily on the approximation of the endocardium by a cylinder. Specifically, that portion of the endocardium covered by the Purkinje network must be approximated by a cylinder. In our work with a rabbit and a canine ventricular data set, we found this approximation to be reasonable and to yield good results. The approximation worked best in the left ventricles of both ventricular structures. The approximation was acceptable in the right ventricles, but there were regions of the surface that were poorly approximated by the chosen cylinders. In our work, we were able to apply the texture-mapping procedure to obtain networks that agreed well with experimental observations. In other data sets, this approximation may not be sufficient to texture-map the ventricles.

Orientation of Ventricles The cylindrical approximation of the ventricles requires the alignment of the cylinder axis with one of the main coordinate axes of the computational box in which the anatomical structure is embedded. Some data sets may not be oriented appropriately to readily allow the approximation of the ventricles by cylinders. One possible means of overcoming this problem is the resampling of the anatomical structure through a rotational transformation.

Structure Resolution and Numerical Methods The full extent of the Purkinje network is not known; our work dealt with the network structure that was readily captured in high-resolution photographs obtained through experimental dissection, but small Purkinje fibers may not be captured in such photographs. Microscopic features of the Purkinje network may exist and may prove to be important to modeling efforts.

Finite-difference methods have inherent length-scale limitations associated with their grid spacing. In our work with macroscopic Purkinje structures we faced issues with representing structures with fine detail on comparatively coarse grids, and so representing even finer-detail networks may pose a significant problem to advancing these methods.

6.2 Future Work

There are many avenues to improving the methods we have developed. We have divided suggestions for future improvements into two categories: suggestions for the optimization of the methods and

procedures developed here, and suggestions for the extension of the methods.

6.2.1 Optimizing Methods

Without changing the core methods presented here, there are several ways by which improvements might be made.

Purkinje Network Digitization The process of digitizing the Purkinje networks from experimental photographs was done manually in our work. An automated procedure for extracting the Purkinje structure might capture features that were undetected in the manual digitization.

The dissection method by which, in particular, the right canine ventricle was dissected resulted in the disconnection of the Purkinje network. Thus fiber ends on one 'side' of the flattened ventricle should correspond with fiber ends on the other 'side'. We ignored this effect in the digitization of the Purkinje networks. A possible avenue for improvement in the Purkinje digitization process is the use of image stitching algorithms to connect these broken network connections.

Selection of Approximating Cylinders The texture-mapping procedure outlined in Section 4 relies on approximating the target surface with a cylinder. In our work, we relied on manual selection of the cylinder. An automated or semi-automated procedure in which a 'best' approximating cylinder is chosen is a natural next step in improving texture mapping results.

Parameter Tuning and the Curvilinear Coordinate System Following the selection of an approximating cylinder based on a chosen curve C, a vector field $\vec{V}$ is defined and a curvilinear coordinate system is induced. The definition of the vector field $\vec{V}$ depends in our definition on a parameter $P > 0$ that controls features of the solution trajectories of a particle traveling in the vector field $\vec{V}$; a more in-depth discussion of the effect of this parameter can be found in section 4.3. We did not investigate the effects of this control parameter extensively nor did we attempt to optimize values of P for our purposes; rather, we performed the procedure with several values and selected the parameter value that produced texture mappings with minimal distortion. More careful selection of the parameter value likely will result in less distortion of the texture image when projected onto the target surface.

6.2.2 Extending Methods

Several extensions of the current work may yield improved results or extend the usefulness or applicability of our methods.

Arbitrary Approximation Surfaces In the texture-mapping procedure, we begin by approximating the target surface with an approximating cylinder. In principle, our method should be extensible to arbitrary approximating surfaces. The key differences in the procedure are the following:

1. Instead of selecting an approximating cylinder with base given by a chosen curve C, an approximating surface S is selected.
2. The vector field $\vec{V}$ previously defined over $\mathbb{R}^2$ is now defined over $\mathbb{R}^3$ and interpolates the outward-pointing unit normal vector to the *surface* S rather than to a curve.
3. Solution trajectories are computed to the vector field $\vec{V}$. Now, solution trajectories are paths in $\mathbb{R}^3$ rather than $\mathbb{R}^2$, so presumably many more solution trajectories will need to be computed.

One of the key benefits of utilizing an approximating cylinder was that the resulting three-dimensional curvilinear coordinate system would merely be the extension of a two-dimensional curvilinear coordinate system, much like how cylindrical coordinates are an extension of polar coordinates. Given an arbitrary approximating surface, the induced curvilinear coordinate system will not have this feature and will be more akin to spherical coordinates.

Utilization of the Curvilinear Coordinate System to Model Non-Superficial Purkinje Networks Our modeling strategy relies heavily on the species-specific fact that the Purkinje network is superficial to the endocardium, and we can therefore reconstruct it by projecting digitized networks onto the endocardium. In some species, such as ungulate species, the Purkinje network is not confined to the endocardium; instead, the Purkinje network resides partially on the endocardium but also within the transmural thickness of the ventricle walls [6, 25].

Using our current methods, it would be straightforward to construct a Purkinje network that resides in a thin mid-myocardial layer between the epicardium and endocardium. A further and more sophisticated extension of our work could be the use of the t-coordinate of the induced curvilinear

coordinate system to add variability of transmural depth to the mapped Purkinje network. This could provide a basis for studying non-superficial Purkinje networks; though at present observations of such networks are limited, and so the exact transmural variation and other structural features of such networks is unknown.

Tuning of the 3D-2D Model through Diffusivity A natural question in the comparison of the 3D-3D and 3D-2D models is whether the two models produce similar results, particularly in the ventricles. We have seen that results can be quite similar. It may be possible to bring the results of the two models closer in line with one another by introducing variable diffusivity into the 2D Purkinje models in the 3D-2D model. This modified diffusivity should most likely be based on some measure of discrepancy between the ventricular surface and the surface chosen to approximate it in the texture-mapping procedure. If the target surface lies within the approximating surface (and is thus 'smaller' locally), then the diffusivity would be increased. Conversely, if the target surface lies outside of the approximating surface (and is thus 'larger' locally), then the diffusivity should be decreased. Of course, some measure of how far the target surface deviates from the approximating surface should be used in the definition of this variable diffusivity.

Alternative Approach for Modeling the Purkinje Structure We have presented two methods for representing the Purkinje network structure: one in which the network is embedded in two-dimensional space, and one where it is embedded in three-dimensional space. The Purkinje network in reality is a collection of fibers that can be idealized as one-dimensional. Thus another avenue for representing the Purkinje network is through a collection of coupled cables.

6.3 Conclusion

We presented a novel method for reconstructing the three-dimensional Purkinje network structure. The method directly uses imaging data taken from experiments and is the first such effort to model the three-dimensional Purkinje network structure. Previous studies that involved the construction of a Purkinje network either did so as a component of other work and did not focus on the construction procedure, were not based directly on experimental data, or generated artificial networks.

Our method makes possible the recovery of Purkinje network structures that are compatible with

real anatomical ventricular structures, enabling the creation of models for the combined system. We have presented the first ventricular-Purkinje structural models where both the ventricles and Purkinje network were based directly on imaging data taken from experiments. We implemented two of these models and were able to reproduce in simulation ventricular activation sequences that closely match experimental observations.

Our model implementations depolarize the ventricles solely through the Purkinje network, and achieve realistic activation times and an activation sequence that agrees well with experimental observations. This suggests that our models and modeling approach accurately captures essential characteristics of the ventricular conduction system.

The development of these models is an important step forward in the investigation cardiac arrhythmias. Our work should be applicable to studying the contributions of the Purkinje network to ventricular arrhythmias.

References

[1] S. Abboud, O. Berenfeld, and D. Sadeh. Simulation of high-resolution QRS complex using a ventricular model with a fractal conduction system. effects of ischemia on high-frequency QRS potentials. *Circulation Research*, 68(6):1751–1760, June 1991. PMID: 2036723.

[2] Omer Berenfeld and Jos Jalife. Purkinje-muscle reentry as a mechanism of polymorphic ventricular arrhythmias in a 3-dimensional model of the ventricles. *Circulation Research*, 82(10):1063–1077, June 1998. PMID: 9622159.

[3] Martin J Bishop, Gernot Plank, Rebecca A B Burton, Jrgen E Schneider, David J Gavaghan, Vicente Grau, and Peter Kohl. Development of an anatomically detailed MRI-derived rabbit ventricular model and assessment of its impact on simulations of electrophysiological function. *American journal of physiology. Heart and circulatory physiology*, 298(2):H699–718, February 2010. PMID: 19933417 PMCID: PMC2822578.

[4] W. J. Boettinger, J. A. Warren, C. Beckermann, and A. Karma. Phase-field simulation of solidification1. *Annual Review of Materials Research*, 32(1):163–194, 2002.

[5] G. Buzzard, J. Fox, and F. Siso-Nadal. Sharp interface and voltage conservation in the phase field method: Application to cardiac electrophysiology. *SIAM Journal on Scientific Computing*, 30(2):837–854, January 2008.

[6] Enrico D Canale. *Cardiac muscle*. Springer-Verlag Berlin, 1986.

[7] Elizabeth M. Cherry and Flavio H. Fenton. Contribution of the purkinje network to wave propagation in the canine ventricle: insights from a combined electrophysiological-anatomical model. *Nonlinear Dynamics*, 68(3):365–379, May 2012.

[8] R. H. Clayton, O. Bernus, E. M. Cherry, H. Dierckx, F. H. Fenton, L. Mirabella, A. V. Panfilov, F. B. Sachse, G. Seemann, and H. Zhang. Models of cardiac tissue electrophysiology: Progress, challenges and open questions. *Progress in Biophysics and Molecular Biology*, 104(13):22–48, January 2011.

[9] C.J. Clements and E.J. Vigmond. Construction of a cardiac conduction system subject to extracellular stimulation. In *Engineering in Medicine and Biology Society, 2005. IEEE-EMBS 2005. 27th Annual International Conference of the*, pages 4235–4238, January 2005.

[10] Derek J Dosdall, Paul B Tabereaux, Jong J Kim, Gregory P Walcott, Jack M Rogers, Cheryl R Killingsworth, Jian Huang, Peter G Robertson, William M Smith, and Raymond E Ideker. Chemical ablation of the purkinje system causes early termination and activation rate slowing of long-duration ventricular fibrillation in dogs. *American journal of physiology. Heart and circulatory physiology*, 295(2):H883–889, August 2008. PMID: 18586887 PMCID: PMC2519198.

[11] Dirk Durrer, R. Th Van Dam, G. E. Freud, M. J. Janse, F. L. Meijler, and R. C. Arzbaecher. Total excitation of the isolated human heart. *Circulation*, 41(6):899–912, June 1970. PMID: 5482907.

[12] Flavio Fenton and Elizabeth Cherry. Models of cardiac cell. *Scholarpedia*, 3(8):1868, 2008.

[13] Flavio Fenton and Alain Karma. Vortex dynamics in three-dimensional continuous myocardium with fiber rotation: Filament instability and fibrillation. *Chaos (Woodbury, N.Y.)*, 8(1):20–47, March 1998. PMID: 12779708.

[14] Flavio H Fenton, Elizabeth M Cherry, Alain Karma, and Wouter-Jan Rappel. Modeling wave propagation in realistic heart geometries using the phase-field method. *Chaos (Woodbury, N.Y.)*, 15(1):13502, March 2005. PMID: 15836267.

[15] Martin Fink, Steven A Niederer, Elizabeth M Cherry, Flavio H Fenton, Jussi T Koivumki, Gunnar Seemann, Rdiger Thul, Henggui Zhang, Frank B Sachse, Dan Beard, Edmund J Crampin, and Nicolas P Smith. Cardiac cell modelling: observations from the heart of the cardiac physiome project. *Progress in biophysics and molecular biology*, 104(1-3):2–21, January 2011. PMID: 20303361.

[16] D W Frazier, P D Wolf, J M Wharton, A S Tang, W M Smith, and R E Ideker. Stimulus-induced critical point. mechanism for electrical initiation of reentry in normal canine myocardium. *Journal of Clinical Investigation*, 83(3):1039–1052, March 1989. PMID: 2921316 PMCID: PMC303781.

[17] Takashi Ijiri, Takashi Ashihara, Takeshi Yamaguchi, Kenshi Takayama, Takeo Igarashi, Tatsuo Shimada, Tsunetoyo Namba, Ryo Haraguchi, and Kazuo Nakazawa. A procedural method for modeling the purkinje fibers of the heart. *The journal of physiological sciences: JPS*, 58(7):481–486, December 2008. PMID: 18926006.

[18] M J Janse, F J Wilms-Schopman, and R Coronel. Ventricular fibrillation is not always due to multiple wavelet reentry. *Journal of cardiovascular electrophysiology*, 6(7):512–521, July 1995. PMID: 8528486.

[19] A. V. Panfilov K H W J Ten Tusscher. Modelling of the ventricular conduction system. *Progress in biophysics and molecular biology*, 96(1-3):152–70, 2008.

[20] Alain Karma. Spiral breakup in model equations of action potential propagation in cardiac tissue. *Physical Review Letters*, 71(7):1103–1106, August 1993.

[21] Jukka Nenonen Kim Simelius. Modeling cardiac ventricular activation. *International Journal of Bioelectromagnetism*, 3:51–58, 2001.

[22] C H Luo and Y Rudy. A model of the ventricular cardiac action potential. depolarization, repolarization, and their interaction. *Circulation research*, 68(6):1501–1526, June 1991. PMID: 1709839.

[23] Colleen C. Mitchell and David G. Schaeffer. A two-current model for the dynamics of cardiac membrane. *Bulletin of Mathematical Biology*, 65(5):767–793, September 2003.

[24] P M Nielsen, I J Le Grice, B H Smaill, and P J Hunter. Mathematical model of geometry and fibrous structure of the heart. *The American journal of physiology*, 260(4 Pt 2):H1365–1378, April 1991. PMID: 2012234.

[25] Noriaki Ono, Takeshi Yamaguchi, Hajime Ishikawa, Mitsue Arakawa, Naohiko Takahashi, Tetsunori Saikawa, and Tatsuo Shimada. Morphological varieties of the purkinje fiber network in mammalian hearts, as revealed by light and electron microscopy. *Archives of histology and cytology*, 72(3):139–149, 2009. PMID: 20513977.

[26] Charles S. Peskin. Fiber architecture of the left ventricular wall: An asymptotic analysis. *Communications on Pure and Applied Mathematics*, 42(1):79–113, January 1989.

[27] P Siregar, J P Sinteff, N Julen, and P Le Beux. An interactive 3D anisotropic cellular automata model of the heart. *Computers and biomedical research, an international journal*, 31(5):323–347, October 1998. PMID: 9790739.

[28] Madison S. Spach, J. Francis Heidlage, Roger C. Barr, and Paul C. Dolber. Cell size and communication: Role in structural and electrical development and remodeling of the heart. *Heart Rhythm*, 1(4):500–515, October 2004.

[29] Carey Stevens, Espen Remme, Ian LeGrice, and Peter Hunter. Ventricular mechanics in diastole: material parameter sensitivity. *Journal of Biomechanics*, 36(5):737–748, May 2003.

[30] Carolyn Eyster Thomas. The muscular architecture of the ventricles of hog and dog hearts. *American Journal of Anatomy*, 101(1):17–57, July 1957.

[31] Frederick J. Vetter and Andrew D. McCulloch. Three-dimensional analysis of regional cardiac function: a model of rabbit ventricular anatomy. *Progress in Biophysics and Molecular Biology*, 69(23):157–183, March 1998.

[32] Edward J. Vigmond and C. Clements. Construction of a computer model to investigate sawtooth effects in the purkinje system. *IEEE Transactions on Biomedical Engineering*, 54(3):389–399, March 2007.